Published in final edited form as:
Exp Eye Res. 2008 August ; 87(2): 147–158. doi:10.1016/j.exer.2008.05.009.

Ultrastructural analysis of damage to nuclear fiber cell membranes in advanced age-related cataracts from India

M. Joseph Costello[1], **Sönke Johnsen**[2], **Sangeetha Metlapally**[1], **Kurt O. Gilliland**[1], **Balasubramanya Ramamurthy**[3], **Pravin V. Krishna**[3], and **Dorairajan Balasubramanian**[3]

1*Department of Cell and Developmental Biology, University of North Carolina at Chapel Hill, Chapel Hill, NC*

2*Department of Biology, Duke University, Durham, NC*

3*LV Prasad Eye Institute, Hyderabad, India*

Abstract

The primary goal was to characterize the structural alterations that occur at the fiber cell interfaces in nuclei of fully opaque cataracts removed by extracapsular cataract surgery in India. The dark yellow to brunescent nuclei, ages 38–78 years, were probably representative of advanced age-related nuclear cataracts. Thick tissue slices were fixed, en bloc stained and embedded for transmission electron microscopy. Stained thin sections contained well-preserved membranes and junctions, although the complex cellular topology often made it necessary to tilt the grid extensively to visualize the membranes. Damage to the fiber cell membranes was noted in all regions of the nucleus. The most important damage occurred within undulating membrane junctions where the loss of membrane segments was common. These membrane breaks were not sites of fusion as membrane edges were detected and cytoplasm appeared to be in contact with extracellular space, which was enlarged in many regions. Dense deposits of protein-like material were frequently observed within the extracellular space and appeared to be similar to protein in the adjacent cytoplasm. The deposits were often 20–50 nm thick, variable in length and located on specific sites on plasma membranes and between clusters of cells or cell processes. In addition, low density regions were seen within the extracellular space, especially within highly undulating membranes where spaces about 100 nm in diameter were observed. The membrane damage was more extensive and extracellular spaces were larger than in aged transparent donor lenses. Because high and low density regions contribute equally to the fluctuations in refractive index, the changes in density due to the observed damage near membranes are likely to produce significant light scattering based on theoretical analysis. The dimensions of the fluctuations in the range 20–100 nm imply that the scattering is probably similar to that of small particles that would increase high-angle scattering visible in the slit lamp. Such damage to membranes would be expected to contribute to the total opacification of the nucleus as the cataract matures. The main sources of the fluctuations appear to be the degradation of membranes and adjacent cytoplasmic proteins, as well as the redistribution of proteins and fragments.

Correspondence to: M. Joseph Costello, PhD, Department of Cell and Developmental Biology, University of North Carolina at Chapel Hill, Chapel Hill, NC 27599-7090; Phone: (919) 966-6981; Fax: (919) 966-1856; email: mjc@med.unc.edu.

Keywords

human nuclear cataract; age-related cataract; electron microscopy; membranes; intercellular junctions; membrane scattering theory

Introduction

Damage to fiber cell membranes has been implicated in the formation of many types of cataracts. Sugar and other osmotic cataracts produce cellular damage that results from the swelling and disruption of fiber cells leading to the accumulation of vesicles, globules and multilamellar membrane cellular debris (Al-Ghoul and Costello, 1993; Creighton et al., 1978; Jongebloed et al., 1988; Kalicharan et al., 1993; Kinoshita et al., 1962; Kuwabara et al., 1969). The accumulation of membranes as cellular debris has also been reported in the posterior subcapsular region of cataracts from patients with retinitis pigmentosa (Dilley et al., 1976), where massive clustering of highly undulating membranes forms distinctive geometrical patterns probably caused by the loss of the cell cytoplasm and redistribution of membrane components. Highly undulating membranes have been observed in age-related nuclear cataracts (Costello et al., 1992) and in the Emory mouse model for nuclear cataracts (Kuck, 1990; Lo and Kuck, 1987). Thus the presence of highly undulating membranes has become a hallmark for nuclear cataract formation. However, the formation of membrane undulations in mammalian lenses occurs naturally during the maturation of nuclear fiber cells (Kuwabara, 1975; Lo and Harding, 1984) and has been reported for many species. Specifically, aged transparent (non-cataractous) human lens nuclei have undulating membrane surfaces within each developmental region that increase in amplitude and complexity toward the nuclear core (Taylor et al., 1996). These undulating membranes do not seem to be correlated with disrupted cells and cellular debris as in cortical cataracts. In fact, there is an inverse correlation between the distribution of cellular damage and the amount of light scattering in age-related nuclear cataracts, with less cellular debris seen toward the center despite increased scattering from the lens center as seen in slit lamp images (Al-Ghoul et al., 1996). Therefore, an understanding of how fiber cell membrane damage produces increased light scattering in cataracts depends on a more detailed knowledge of the composition and ultrastructure of the membranes.

All fiber cells are interconnected by an extensive array of gap junctions that provide intercellular pathways for the transport of water and other small molecules less than about 1 kDa (Goodenough, 1992; Goodenough et al., 1996; White and Bruzzone, 2000). Although this feature is similar to other epithelial tissues, the gap junctions between human lens fiber cells have two types of connexins, Cx46 and Cx50, that form the connexon hemichannels, with Cx46 found mainly in the cortex and outer nuclear layers and Cx50 mainly found in the nuclear core (Chung et al., 2007; Tenbroek et al., 1992; White et al., 1998). Compared to other epithelia, gap junctions in the lens have a smaller extracellular gap, which is about 1nm and not resolved in thin-section transmission electron microscopy (TEM), thus presenting a pentalamellar profile about 16 nm in overall thickness (Peracchia et al., 1985). This structural feature is consistent throughout the cortex and nucleus and does not appear to change with mammalian species, age or nuclear cataract formation (Costello et al., 1989; Costello et al., 1992; Kuszak and Costello, 2004; Zampighi et al., 1989). Within the plane of the membrane, paired connexons form plaques in which individual junctional channels are packed in dense irregular arrays as seen in freeze-fracture images (Benedetti et al., 2000; Costello et al., 1985, 1989; Kistler and Bullivant, 1980; Kuszak et al., 1982; Vrensen et al., 1990, 1992; Zampighi et al., 1982, 1989; Zampighi, 2003).

Aquaporin 0 (AQP0, formerly MIP or MP26), the most abundant protein in the lens fiber cell membrane, is a member of the water transport family of integral channel proteins (Agre,

2004). Based on high-resolution x-ray and electron crystallographic analysis, the 28.2 kDa monomer has four transmembrane alpha-helices and two segments that dip half-way from opposite sides to form a portion of the wall of the narrow channel (Gonen et al., 2004, 2005; Harries et al., 2004; Murata et al., 2000; Walz et al., 1997). Within the eye, AQP0 is found exclusively in lens fiber cells, whereas other members of the water transport family are found in the lens epithelium and other ocular structures (Hamann et al., 1998; Verkman, 2003). Structural evidence also shows that AQP0 is a tetramer and is inserted into cortical fiber cell membranes as 7–8 nm diameter particles composed of four orthogonally associated monomers (Costello et al., 1985; Verbavatz et al., 1993; Zampighi et al., 2003). It has been suggested that the main function of AQP0 in fiber cells is to transport water from the extracellular space (ECS) to the cytoplasm, thus minimizing the ECS, an inherently low refractive index medium (Costello et al., 1989; Zampighi et al., 1989). Some doubts about this proposed function were raised when physiological measurements clearly showed that AQP0 transports water very poorly compared to other aquaporins (Chandy et al., 1997; Yang and Verkman, 1997). This documented low water transport is perhaps offset by the high density of AQP0, which is about one or two orders of magnitude greater than aquaporins in any other tissue. In addition to channel functions, fiber cell membranes have specialized AQP0 – lipid interactions that determine the cell shape, surface topology, intercellular junctions and important features of membrane aging and cataract formation (Kuszak and Costello, 2004).

Within the lens cortex, AQP0 aggregates into plaques with a regular square array of 6.6 nm repeat (Buzhynskyy et al., 2007; Zampighi et al., 1982). These plaques can align and adhere across the ECS to produce junctions that have pentalamellar profiles in TEM thin sections similar to fiber cell gap junctions, except the junctions are about 14 nm thick, and were termed thin symmetric junctions (TSJs) to emphasize the similarity to gap junctions (Costello et al., 1989). Although alignment of water channels between crystalline layers of membranes is possible, initial reports suggested that the channels were not aligned indicating that the close membrane association was an adherens junction (Costello et al., 1989; Fotiadis et al., 2000). Support for this interpretation has come from high resolution electron crystallographic analyses of reconstituted 2D arrays of AQP0 from sheep nuclei showing paired membranes with closed water transport pathways of AQP0 monomers and specific bonding across the ECS that held the sheets of proteins in close contact in vitro (Gonen et al., 2004, 2005). The formation of crystalline arrays of AQP0 in cortical membranes in vivo diminishes the number of mobile AQP0 particles and clears some membranes of integral protein particles. The large sheets of membrane pairs appear to redistribute in the cortex coincident with the production of curved membranes containing the arrays of AQP0. It has been hypothesized that, as the cytoskeleton is removed during the last stages of cellular differentiation within the cortex (Alcala and Maisel, 1985; Quinlan et al., 1999), the integral proteins of the relatively flat membranes of the cortex lose their contacts with the cytoskeleton (Lindsey Rose et al., 2006) and, without constraints, reorganize to minimize surface energy (Kuszak and Costello, 2004). The curved crystalline arrays then pair with the protein-poor lipid bilayers to create a new junctional association that is thin and asymmetric, pairing 7 nm thick curved AQP0 arrays with 4–5 nm thick bilayers, to produce junctions about 11 nm thick that have been termed square array junctions (SAJs) (Costello et al., 1985, 1989; Lo and Harding, 1984). In young lenses SAJs dominate the surface topology of nuclear fiber cells producing the undulating polygonal arrays of furrowed membranes (Dickson and Crock, 1972; Kuszak et al., 1988; Vrensen et al., 1992).

Oxidation in general and lipid peroxidation specifically have been shown to modify lipids, integral membrane proteins and associated cytoplasmic proteins (Babizhayev, 1996; Borchman et al., 2000; Garner et al., 1981; Spector, 1984). For human age-related nuclear cataracts, it has been proposed that the initial site of membrane damage is at the protein-poor lipid bilayer within the complex undulating membranes of the aged nuclear fiber cells (Costello et al., 1992). As noted above, these lipid bilayers appear during the redistribution of integral proteins

to form gap junction plaques and square arrays of AQP0, as adjacent fiber cells become closely associated in the lens nucleus (Kuszak and Costello, 2004). The hypothesis is that the patches of lipid bilayer are potentially weak points in the membrane and possibly the least capable of withstanding long-term oxidative stress. The morphological evidence that some of these bilayer regions are lost comes from high magnification transmission electron micrographs showing gaps in the membrane profiles and from the deposition of protein-like material in the ECS (Al-Ghoul and Costello, 1993; Al-Ghoul et al., 1996; Costello et al., 1992). These earlier studies of membrane ultrastructure in age-related nuclear and diabetic cataracts were performed on material extracted in the early stages of nuclear cataract formation. The main goal of this study was to determine the extent of membrane damage in nuclei of advanced or totally opaque cataracts from patients in India who were blind prior to cataract extraction. In addition a theoretical analysis is introduced to estimate the contribution of membrane damage to opacification.

Materials and Methods

Lenses

Lens nuclei were obtained from the operating room suite at the LV Prasad Eye Institute (Hyderabad, India) shortly after extracapsular extraction of cataractous nuclei from patients who were blind due to cataracts. The nuclear buttons were collected with a limited amount of information including age, gender and clinical cataract grade. A typical specimen is presented (Fig. 2) from an age range of 38–75 years (average 61 ± 12 years, n = 15) and average diameter 7.6 ± 0.7 mm (n = 15). For comparison transparent lenses from donor eyes were collected within 12 hours of death with an age range of 48–78 years (average 57 ± 12 years, n = 5) and average diameter of 8.3 ± 0.2 mm (n = 5). No patient identifiers were used and no histories were obtained following the tenets of the Declaration of Helsinki using procedures approved by the University of North Carolina Internal Review Board for protection of human subjects.

Transmission electron microscopy

Fourteen advanced nuclear cataracts from non-diabetic patients and two donor lenses were Vibratome sectioned (model 1000, St. Louis, MO) to 200 μm thickness, immersion fixed and processed for transmission electron microscopy (TEM) as described previously (Freel et al., 2002). Briefly, sections were initially fixed for 12–18 h in 2.5% glutaraldehyde, 2% paraformaldehyde and 1% tannic acid in 0.1 M cacodylate buffer (pH 7.2). En bloc staining with osmium tetroxide and uranyl acetate followed by epon embedding ensured good preservation of membranes. Thin sections (50–70 nm) were cut with a diamond knife (Diatome US, Ft. Washington, PA) from mesas raised to include the embryonic nucleus along the optic axis (Fig. 1). Sections were stained with lead citrate and uranyl acetate. All images were of the fetal and embryonic nuclei and were recorded on an FEI Tecnai 12 TEM (FEI, Hillsboro, OR) at 80 kV with a Gatan 1k × 1k CCD camera (model 694, Pleasanton, CA) equipped with Digital Montage software. The sample stage was rotated, often between ±50°, to reveal trilamellar membrane profiles commonly recorded at magnifications of 30,000 to 60,000 times.

Quantitative analysis

The measurement of the average thickness of the extracellular space (ECS) was performed using NIH Image J (W. Rashband, NIH Image J, version 1.39u, http://rsb.info.nih.gov/ij/) equipped with a plug-in to read images generated by Digital Micrograph software (version 3, Gatan, Pleasanton, CA) proprietary image format. Image montages (typically, 3×3 montages at 6,500x to 30,000x) were opened on a Mac Power PC (model Dual 2 GHz G5, operating system 10.4.11, Apple Computer, Cupertino, CA) and converted from 16 bit to 8 bit followed by processing to a binary image with the threshold command. The light ECS was converted to black pixels and when the images contained cells as pictured in Fig. 1, there were only scattered

black specks over the cell cytoplasm. These were removed by two successive dilate / close commands, followed by erode / open commands to return the ECS to its original size giving a nearly continuous black line of variable width. Spaces or openings within the black line due to gap junctions were filled in manually with a thin black line and any remaining black specks not part of the ECS were erased manually. Smeared membranes due to excessive tilting were excluded. The original image was opened on the monitor along with the binary image to ensure that the ECS size was accurate and that the correct identification of membranes and non-ECS structures were made. The adjusted binary image and the original were superimposed (using saved TIFF images in Adobe Photoshop) with variable transparency to confirm the exact correspondence of the ECS black area to the light ECS in the original image. A binary image was then analyzed with Image J by automatically counting the black pixels (using the histogram function) and calculating the fraction of total pixels, which was then used to calculate the actual area of the ECS from the known dimensions of the image. The freehand line command was then used to measure the lengths of all the cell interfaces in the binary image of the ECS. The ECS area was divided by the total length to yield the average thickness of the ECS. Statistical comparisons were made using the student t-test (InStat, version 3.0b, GraphPad Software, San Diego, CA) for which $p < 0.05$ was considered to be significant.

Theoretical analysis

Light incident on a stack of thin, non-absorbing layers will undergo multiple reflections at the various interfaces, which can greatly reduce transmission. Because there are an infinite number of combinations of reflections, a direct calculation is exceedingly tedious even in the case of only one layer. Fortunately, an exact solution can be found using matrix methods developed by Herpin (1947) and Weinstein (1954) (reviewed by Dobrowolski, 1995). Briefly, the fraction of light, *T*, that passes through a stack of layers is given by

$$T=|t|^2,$$

where *t* is the complex amplitude of the transmitted light and is equal to

$$t=\frac{2n_{cyto}}{n_{cyto}E+H}.$$

where n_{cyto} is the refractive index of the cytoplasm. *E* and *H* are the complex amplitudes of the electric and magnetic fields of the transmitted light and are found by multiplying a set of matrices, one for each layer (Fig. 3). In this case, the first and last layers (i.e., the membranes) are equal, so

$$\begin{pmatrix} E \\ H \end{pmatrix}=\begin{pmatrix} \cos\delta_m & \frac{i}{n_m}\sin\delta_m \\ \mathrm{in}_m \sin\delta_m & \cos\delta_m \end{pmatrix}\cdot\begin{pmatrix} \cos\delta_e & \frac{i}{n_e}\sin\delta_e \\ \mathrm{in}_e \sin\delta_e & \cos\delta_e \end{pmatrix}\cdot\begin{pmatrix} \cos\delta_m & \frac{i}{n_m}\sin\delta_m \\ \mathrm{in}_m \sin\delta_m & \cos\delta_m \end{pmatrix}\cdot\begin{pmatrix} 1 \\ n_{cyto} \end{pmatrix},$$

where $\delta_m=\frac{2\pi}{\lambda}n_m d_m$ and $\delta_e=\frac{2\pi}{\lambda}n_e d_e$. The variables n_m and n_e are the refractive indices and d_m and d_e are the thicknesses of the membrane and extracellular spaces, respectively. λ is the wavelength of the incident light *in vacuo*.

If the light path through the lens intercepts k sets of these three-layer interfaces (membrane-ECS-membrane), the transmittance for the whole lens is simply

$$T_{lens}=T^k.$$

It is important to note that we assumed that all the interfaces were perpendicular to the incident light. Light striking the interfaces at more glancing angles (>~45°) will be more strongly reflected, reaching 100% near parallel angles of incidence. Because some of the interfaces in

the lens will have these high angles, our calculations are a conservative estimate. The matrix calculations were solved and the results were plotted using MATLAB (Natick, MA).

Results

Membrane damage

Membrane damage has been characterized in the oldest cells of advanced nuclear cataracts from India. These dense cataractous nuclei have in common the deep yellow to brunescent pigmentation and nearly total scatter or absorption of light (Fig. 2). Even the two nuclei graded 3 could pass only a small amount of light and could not form an image of a meshwork through the nuclei. The question arises whether these nuclei have extensive cell and membrane damage in the central nuclear core where age-related nuclear cataracts normally begin as a diffuse scattering. To address these issues, it was necessary to employ techniques that were capable of preserving membrane ultrastructure, and to make comparisons among cataracts and with transparent donor lenses. A low magnification overview from an advanced cataract (Fig. 4A) is similar to that from an equivalent region of an adult transparent donor lens (Fig. 4B). The cells have large irregular cross-sections and are irregularly packed, typical of the deep fetal and embryonic nuclei (Taylor et al., 1996). The white lines at low magnification represent the cell interfaces including the paired plasma membranes and the ECS. The integrity of the membranes could be appreciated only at high magnification (Fig. 5). A representative interface from a nuclear cataract (Fig. 5A) displays several types of junctions including two segments of gap junctions (Fig. 5A, red arrows) and undulating membranes (Fig. 5A, blue arrowheads). The ECS is irregular in shape and well defined between two apposing plasma membranes in only a few places. It is important to note that deposits of material occur within the ECS frequently (Fig. 5A, yellow) and that these deposits stain similarly to the proteins within the surrounding cytoplasm. It is also noted that many deposits occur specifically on the curved portions of undulating membranes that are convex with respect to the adjacent cytoplasm (Fig. 5A, yellow). Similar patterns of membranes, junctions and deposits are seen in a different cataractous nucleus compared to a similar region in a transparent donor nucleus (Fig. 5B and C). Notice that the cytoplasm in these images has variable texture, with the donor lens having the most homogeneous texture (Fig. 5C), and that all are composed of globular subunits (Metlapally et al., 2008). The cytoplasmic proteins pack closely to the cytoplasmic surfaces of the junctional and non-junctional membranes (Fig. 5).

Membranes at intersections of cells and cell processes

The intersections of cells and cell edge processes (Fig. 6A, EP) have complex topology (Taylor et al., 1996). The trigonal cellular intersections are numerous. At each point of the typical flattened hexagonal fiber cell in the lens cortex, three cells come together. The flat surfaces between adjacent cortical fiber cells (four narrow faces and two broad faces) normally have very close association of plasma membrane pairs and minimal ECS. In the nucleus of an adult human lens the fiber cells can have a very complex non-hexagonal shape, although the trigonal cellular contacts are maintained. Moreover, the numerous edge processes (finger-like processes) found between adjacent plasma membranes also have trigonal intersections all along their length as the plasma membranes come together on either side of the edge processes. This is illustrated for typical fiber cells from the fetal and embryonic nuclei (Fig. 6). These intersections in 3D are perhaps extended channels or small canaliculi bounded by plasma membranes. At high magnification these intersections can often be seen to contain protein-like material in the ECS (Fig. 6B and C). These look similar structurally to the ECS deposits on the curved membranes between intersection points (Fig. 6B and C); however, there is no evidence that they have the same composition or origin as the ECS deposits on the membranes. The material in the trigonal points probably provides structural support similar to extracellular matrix proteins in other epithelia.

Enhanced visualization of membranes with grid tilt

Membranes are difficult to visualize even at high magnification. It is often essential to tilt the thin section extensively in the TEM to bring the membrane profiles into view. The fiber cell surface topology is so complex that rarely are the membranes in the ideal orientation around the perimeter of a fiber cell cut in cross-section (see Fig. 1). Moreover, because nuclear fiber cell membranes are difficult to preserve, the absence of membranes in most high-magnification views of fiber cells is often interpreted as poor membrane preservation. If full rotation of a thin-section were available (requiring rotation about many axes), then the true extent of the preserved membranes could be determined and it would be obvious that far more membranes are preserved than is visible in any one TEM image. The influence of tilt can be illustrated by examining a finger-like projection, which is surrounded by a plasma membrane pair as in a whole cell but is much smaller and can be visualized in single images at high magnification. The finger-like projection (Fig. 7A) at 0° tilt shows less than 50% of surrounding membranes (blue and green lines). At −40° tilt (Fig. 7B) there are about 20% more membranes visible and viewing at multiple angles shows that at least one plasma membrane is present around the entire perimeter. High tilt is also often needed to see thin symmetric (14 nm) junctions within undulating membranes (Fig. 8A, arrows). Optimum tilt can be used to reveal the membrane borders on enlarged extracellular spaces (Fig. 8B, ECS). These are cylindrical low-density regions about 100 nm in diameter that are potentially strong light scattering regions.

Quantitative evaluation of the size of the extracellular space between fiber cells

The ECS in young normal human and animal lenses is very small (Kuszak and Costello, 2004). Over long stretches of cell interface, along the broad and narrow faces, the ECS in the cortex is about 10–15 nm thick and is reduced only at junctions. In the nucleus of young lenses the ECS is consistently smaller and, in many cases, not detectable, because the plasma membranes have formed extensive junctions or are in close non-junctional contact where the contact is about 1 nm and cannot be clearly resolved by thin-section TEM. In aged and cataractous lens nuclei, the ECS was observed to be enlarged (Al-Ghoul et al., 1996; Costello et al., 1992; Taylor et al., 1997). At high magnification the low stain density of the interface contains two plasma membranes (when preserved), the ECS and any deposits, as illustrated from a cataractous embryonic nucleus (Fig. 9A). The light ECS areas appear as nearly continuous regions following binary thresholding and inversion into black pixels to increase visibility (as described in Methods; Fig. 9B). The correspondence of the adjusted binary image of the ECS to the original image is confirmed by superimposing the images (in Adobe Photoshop) and adjusting the color and transparency to highlight the ECS and ECS deposits (Fig. 9C). The histogram function gives the number of pixels or area of the ECS and, dividing by the length of the interface, gives an approximate measure of the ECS average thickness. For the Indian cataract illustrated in Fig. 9, the average ECS thickness was about 42 nm. For a similar region in an aged donor lens, the thickness was about 30 nm. For about 50 μm length of interface in Indian cataractous nuclei, the thickness was 37 ± 3 nm ($n = 5$) and for an equivalent length in donor lens nuclei was 30 ± 2 nm ($n = 5$), which are significantly different at $p < 0.01$. These are approximations to the actual ECS thickness because corrections have not been made for smearing of the ECS due to tilting within the section, although regions in which excess tilt obscured the membranes were not included. The objective of these measurements was to demonstrate that the average width of the ECS can be determined approximately from digital images and that the trend was an increased ECS thickness with cataract formation. A longer length of ECS, a larger sample size of lenses and corrections for smearing of membranes with tilt (using serial section or tomographic reconstructions) are needed to improve the accuracy and to strengthen the statistical significance of the differences between aged donor nuclei and age-related nuclear cataracts.

Theoretical analysis of the predicted scattering from nuclear fiber cell interfaces

Thin film scattering theory is employed to describe the reflectance of thin layers at interfaces in the thin coating industry, for example, in the manufacture of interference filters and anti-reflection coatings of compound microscope and camera lenses. The theory is essentially an exact solution of Maxwell's wave equations and (as mentioned above) can also take into account the dependence on the angle of the light relative to the membranes and polarization effects (Herpin, 1947; Dobrowolski, 1995; Weinstein, 1954). The key parameters are the refractive indices and thicknesses of the layers and the surrounding media. For this application, the scattering is calculated for a specific wavelength of light (550 nm) using dimensions derived from the ultrastructural analysis and literature refractive index values. The scattering for a single membrane-ECS-membrane three-layer interface is very small and for the transparent donor lenses, the passage of light through the nucleus is not greatly influenced by the presence of multiple membrane layers, estimated to be about 4000 layers. Therefore, the reflectance, also a measure of the scattering as light is reflected at different angles, is expressed in terms of percent transmittance, which should approach 100% for transparent lenses. To illustrate the method, the transmittance is calculated for cytoplasmic and ECS refractive indices set at 1.42 (Jones et al., 2005) and 1.35 (Charney and Brackett, 1961), respectively, while the membrane index is varied from 1.40 to 1.55 and the ECS thickness is varied from 1 nm to 100 nm (Fig. 10A). The 3D surface plot shows a very steep rise from ECS spacing about 50 nm to 25 nm, and, importantly, approaches 100% transmittance along the ridge for ECS thickness of 20 – 30 nm. It is interesting that the transmittance drops off as the ECS thickness decreases toward 1 nm thus producing the pointed tail at low ECS. This aspect of the surface is more clearly visualized in the alternative flat display (Fig. 10B), which is identical except the cytoplasmic refractive index is set to 1.40 (Pierscionek, 1997), as might represent the case for aged or cataractous nuclei that have lost some cytoplasmic crystallins. Because the membrane index is probably near 1.50 (Chong and Colbow, 1976), the transmittance increases from about 40% at zero ECS to 100% from about 22 nm to 28 nm ECS. Above 35 nm ECS the transmittance has already dropped to about 85% on the very steep slope suggesting that very small changes in the size of the ECS above 35 nm can have a dramatic effect on the transmittance. The values reported above of 30 nm average ECS for the transparent donor lenses and 37 nm average ECS for the advanced nuclear cataracts corresponds to about 100% and about 85% transmittance on this surface plot (Fig. 10B). These plots illustrate that 100% transmittance occurs when the average index of the 3-layer unit, which is just the indices of the membrane and ECS weighted by their relative thicknesses, equals the index of the cytoplasm (Michael et al., 2003). In other words, if the correct ECS thickness is selected, then the whole 3-layer interface becomes optically invisible.

Discussion

Ultrastructural data are presented showing that the fiber cell membranes and intercellular interfaces are significantly altered in advanced nuclear cataracts from India. Specific and extensive damage to the nuclear fiber cell membranes is reported including the loss of segments of membranes, enlargement of the ECS between membranes and deposits of material in the ECS. It is important that the types of membrane damage are similar to those reported previously for early-stage age-related nuclear cataracts (Al-Ghoul et al., 1996; Costello et al., 1992). The damage to membranes and the amount of material deposited in the ECS seem to be more extensive in the Indian nuclear cataracts compared to age-related nuclear cataracts from the US. This is consistent with the maturity of the Indian cataracts, which were fully opaque or sufficiently dense to limit image formation. Although the types of membrane damage observed are not unique to the Indian nuclear cataracts, the extent of the damage is probably sufficient to contribute to the opacification of the nucleus. It is noted, however, that similar changes have occurred in the aged transparent donor lenses from India. Therefore, the damage to membranes

and fiber cell interfaces begins during the normal aging process before nuclear opacification occurs. This is consistent with the similarity of cellular structure reported for aged transparent lenses and immature nuclear cataracts from the US (Al-Ghoul et al., 1996; Costello and Kuszak, 2007; Gilliland et al., 2004; Kuszak et al., 1998) and the increase in scattering with aging in the general population.

The key types of damage are loss of the protein-poor bilayer segments opposite curved membranes proposed to contain AQP0 arrays (based on previous labeling and structural studies), sufficient enlargement of the ECS to decrease transmittance (Fig. 10) and frequent deposition of protein-like material in the ECS, often on the curved membrane arrays of AQP0 (Fig 11). It is interesting that the deposits are exclusively found on the extracellular side of the plasma membranes, opposite to the suggested cytoplasmic surface for tightly bound alpha-crystallin to lens membranes (Cobb and Petrash, 2002;Ifeanyi and Takemoto, 1989, 1990;Zhang and Augusteyn, 1994). This location of deposits is also inconsistent with earlier suggestions that age-related nuclear cataracts are in part due to the precipitation of crystallins on the cytoplasmic side of membranes triggering protein crosslinking and membrane breakdown (Boyle and Takemoto, 1996;Garner et al., 1981;Spector, 1984). It is possible that these processes occur to some extent but result in a uniform dense association of cross-linked crystallins at membrane cytoplasmic surfaces, as appears to be the case in the nuclear cataracts displayed here. The composition of the ECS deposits is unknown, although the similarity to the staining of crystallins in the adjacent cytoplasm and the naturally occurring extracellular matrix material at trigonal points of cells and edge processes (Costello et al., 1993;Kuszak and Costello, 2004) strongly suggest that the material is composed of crystallins and fragments of crystallins (or possibly remnants of the cytoskeleton or extracellular matrix proteins). Other observations also support this suggestion. First, deposits have been reported to be more numerous in regions adjacent to damaged cells where the cytoplasmic protein is free to diffuse into the ECS, and even out of the lens, as in lenses from diabetic patients (Al-Ghoul and Costello, 1993). Second, the deposits are adjacent to cytoplasm that at high magnification appears to have lost components (producing low-density regions) and is composed of crystallins known to be partially degraded during aging and cataract formation (Hanson et al., 2000;Lampi et al., 1998;Truscott, 2005). Third, the observed loss of membrane segments gives the crystallins and fragments access routes to the ECS. Fourth, many of the changes to crystallins result in increased acidity (such as deamidation, Takata et al., 2007;Takemoto and Boyle, 1999); the increased negative charge causes the deposition onto the curved surfaces of AQP0 arrays because these have a net positive charge resulting from four surface positive charges per monomer (Harries et al., 2004). Fifth, the localization of deposits within the embryonic nucleus, where access to non-protein substances is limited, raises the probability that the deposits are derived from the most abundant material in the vicinity.

The size of the ECS is critical to evaluating the contribution of the modified interfaces to increased light scattering. Regions with low stain density may be filled in vivo with a low refractive index protein solution that would create refractive index fluctuations across the ECS. The remaining membranes and ECS deposits are probably high refractive index media and together these rapid fluctuations in refractive index would produce increased scattering. However, because changes to the fiber cell interfaces begin in aged transparent lenses, there must be a threshold of ECS size and magnitude of fluctuations that creates the excess scattering seen in nuclear cataracts. The estimated average size of the ECS made here for transparent nuclei and advanced cataracts of 30 nm and 37 nm, respectively, are similar. The theoretical analysis reveals that values of ECS near 30 nm are consistent with nearly 100% transmittance and that increasing the ECS in this critical size region by only 10 nm may reduce the transmittance by more than 20% (Fig. 10). Therefore, scattering from alterations at the membrane interfaces may make a significant contribution to the opacification of the nucleus in advanced cataracts. The size of the ECS may be affected by several factors including the

condensation of the cytoplasm during the crosslinking of crystallins and formation of high-molecular-weight aggregates. As the cytoplasm contracts, perhaps in a synergetic process (Bettelheim, 1979;Lizak et al., 2005), water is redistributed and adjacent cells may pull apart. The ECS may also be created as an artifact of fixation and dehydration during processing for TEM. In this case the cytoplasm would be expected to pull away from gap junctions, which is not observed heere (see Fig. 5 and Fig 6). Furthermore, these methods can preserve membranes in animal models where the ECS is minimal and the cytoplasm is in close contact on both sides of the membrane pair separating fiber cells (Costello et al., 1993;Kuszak and Costello, 2004). Recent experiments using high-pressure freezing as the initial fixation, instead of chemical fixation, produced similar preservation of normal and cataractous lenses (Costello, 2006), suggesting that the preparation methods used here faithfully preserve the ECS and the associated membranes.

The proposed loss of membrane segments may be dependent on the unique distribution of lipids. The lipid composition of mammalian lens fiber cells is unusual because the cholesterol content is very high (about 50% of all lipids) and the phospholipids have a high proportion of sphingomyelin (Huang et al., 2005). In humans and other long-lived animals, sphingomyelin is in the form of dihydrosphingomyelin, a saturated laterally bonded and stiff lipid that is resistant to oxidative damage and is probably the most stable lipid known (Borchman et al., 2004). Although the distribution of the lipid components has not been established, a possible association of dihydrosphingomyelin with the AQP0 arrays could produce highly stable and rigid curved membranes. The main remaining phospholipid, phosphatidyl choline, together with cholesterol and other phospholipids, may form the protein-poor lipid bilyers of the undulating membranes. The phosphatidyl choline normally contains double bonds that would be susceptible to lipid peroxidation, which has been shown to occur throughout the nucleus in a rat model (Marsili et al., 2004) and is well-documented in human lenses (Babizhayev, 1996; Borchman and Yappert, 1998; Huang et al., 2006). If these segments of membrane are damaged and lost, there is no source to replenish the lipids deep within the lens nucleus, so the cell integrity would be lost. However, the remaining membranes, composed mainly of gap junction plaques and rigid sheets of crystalline AQP0, preserve the cell shape. Importantly, the crystalline arrays on the undulating membranes probably overlap to create adhesive junctions that help stabilize the membranes and surface topology (Figs. 11).

The adhesive role of junctions containing AQP0 is confirmed in high-resolution crystallographic studies. Using atomic force microscopy, it was shown that extracellular surfaces of 2D crystalline arrays of AQP0 interdigitate in a tongue-and-groove fashion (Fotiadis et al., 2000). This overlap of surface protrusions supports the non-alignment of water channels and the increase of hydrophobic interactions that stabilize the junction. X-ray crystal studies at high resolution of whole AQP0 showed that the water channel was intact (Harries et al., 2004). This junction may form as water is removed from the ECS and is present extensively in the cortex, as demonstrated for bovine lenses (Fig. 11A, labeled TSJ: Costello et al., 1989; Kuszak and Costello, 2004). Within the nucleus the large flat sheets of TSJ give rise to curved membranes that partially overlap. An important modification is that AQP0 is partially cleaved in the nucleus (Ball et al., 2004; Han and Schey, 2004; Schey et al., 2000), which is thought to induce the formation of a different type of adhesive junction. High-resolution TEM analysis of frozen-hydrated crystalline arrays of membrane pairs showed that the AQP0 molecules formed a network of precise contacts of exposed proline residues across the ECS, creating a tight bond between surfaces, and that the water channels were constricted (Gonen et al., 2004, 2005). This adhesive junction may correspond to the TSJ at curvature transitions within undulating membranes (Fig. 5C, 8A arrows, and 11A, arrows). Although the water channels in single membranes and channels in gap junctions may still be functional in the nucleus, these membranes may have a secondary role as adhesive junctions. The proposed membrane breakdown described here and the known fusion of fiber cells in mammalian lenses (Kuszak

et al., 1985; Shestopalov and Bassnett, 2000, 2003), probably create large pathways for the diffusion that may bypass the smaller channels.

In conclusion, membrane damage in advanced nuclear cataracts from India is more extensive than in early stage nuclear cataracts from the US. The ultrastructure of damaged membranes is similar in all age-related nuclear cataracts thus far examined, including loss of membrane segments, enlargement of the extracellular space and deposition of protein-like material in the extracellular space. Fluctuations in refractive index around damaged membranes are typically on a scale less than 100 nm and are predicted to contribute significantly to high-angle scattered light seen in slit lamp images and to retinal stray light. Extensive extracellular space deposits of protein-like material suggests that crystallins and fragments from the cytoplasm have redistributed into the extracellular spaces during cataract formation. In addition to scattering from multilamellar bodies (Gilliland et al., 2008) and textured cytoplasm (Metlapally et al., 2008), the new theoretical treatment suggests that the ECS in Indian lens nuclei may be enlarged enough to contribute to the excess light scattering of advanced nuclear cataracts.

Acknowledgements

We thank Mr. Harold Mekeel and Mr. Kenji Leonard for their expert microscopy assistance. Presented in part at the 2007 Annual Meeting of the Association for Research in Vision and Ophthalmology, Ft. Lauderdale, Florida. This project was supported in part by NIH-NEI Research Grant EY008148 (UNC) and Core Grant EY005722 (Duke University).

References

Agre P. Nobel Lecture. Aquaporin water channels. Biosci Rep 2004;24:127–163. [PubMed: 16209125]

Al-Ghoul KJ, Costello MJ. Morphological changes in human nuclear cataracts of late-onset diabetics. Exp. Eye. Res 1993;57:469–486. [PubMed: 8282033]

Al-Ghoul KJ, Lane CW, Taylor VL, Fowler WC, Costello MJ. Distribution and type of morphological damage in human nuclear age-related cataracts. Exp. Eye. Res 1996;62:237–251. [PubMed: 8690033]

Alcala, J.; Maisel, H. Biochemistry of lens plasma membrane and cytoskeleton. In: Maisel, H., editor. The Ocular Lens: Structure, Function and Pathology. New York: Marcel Dekker; 1985. p. 169-222.

Babizhayev MA. Failure to withstand oxidative stress induced by phospholipid hydroperoxides as a possible cause of the lens opacities in systemic diseases and ageing. Biochim. Biophys. Acta 1996;1315:87–99. [PubMed: 8608175]

Ball LE, Garland DL, Crouch RK, Schey KL. Post-translational modifications of aquaporin 0 (AQP0) in the normal human lens: spatial and temporal occurrence. Biochemistry 2004;43:9856–9865. [PubMed: 15274640]

Benedetti EL, Dunia I, Recouvreur M, Nicolas P, Kumar NM, Bloemendal H. Structural organization of gap junctions as revealed by freeze-fracture and SDS fracture-labeling. Eur J Cell Biol 2000;79:575–582. [PubMed: 11001494]

Bettelheim FA. Syneresis and its possible role in cataractogenesis. Exp. Eye. Res 1979;28:189–197. [PubMed: 446561]

Borchman D, Giblin FJ, Leverenz VR, Reddy VN, Lin LR, Yappert MC, Tang D, Li L. Impact of aging and hyperbaric oxygen in vivo on guinea pig lens lipids and nuclear light scatter. Invest. Ophthalmol. Vis. Sci 2000;41:3061–3073. [PubMed: 10967065]

Borchman D, Yappert MC. Age-related lipid oxidation in human lenses. Invest Ophthalmol Vis Sci 1998;39:1053–1058. [PubMed: 9579487]

Borchman D, Yappert MC, Afzal M. Lens lipids and maximum lifespan. Exp Eye Res 2004;79:761–768. [PubMed: 15642313]

Boyle DL, Takemoto L. EM immunolocalization of alpha-crystallins: association with the plasma membrane from normal and cataractous human lenses. Curr. Eye. Res 1996;15:577–582. [PubMed: 8670759]

Buzhynskyy N, Hite RK, Walz T, Scheuring S. The supramolecular architecture of junctional microdomains in native lens membranes. EMBO Reports 2007;8:51. [PubMed: 17124511]

Chandy G, Zampighi GA, Kreman M, Hall JE. Comparison of the water transporting properties of MIP and AQP1. J. Membr. Biol 1997;159:29–39. [PubMed: 9309208]

Charney E, Brackett FS. The spectral dependence of scattering from a spherical alga and its implications for the state of organization of the light-accepting pigments. Arch. Biochem. Biophys 1961;92:1–12. [PubMed: 13692507]

Chong CS, Colbow K. Light scattering and turbidity measurements on lipid vesicles. Biochim Biophys Acta 1976;436:260–282. [PubMed: 1276217]

Chung J, Berthoud VM, Novak L, Zoltoski R, Heilbrunn B, Minogue PJ, Liu X, Ebihara L, Kuszak J, Beyer EC. Transgenic overexpression of connexin50 induces cataracts. Exp Eye Res 2007;84:513–528. [PubMed: 17217947]

Cobb BA, Petrash JM. alpha-Crystallin chaperone-like activity and membrane binding in age-related cataracts. Biochemistry 2002;41:483–490. [PubMed: 11781086]

Costello MJ. Cryo-electron microscopy of biological samples. Ultrastruct. Pathol 2006;30:361–371. [PubMed: 17090515]

Costello, MJ.; Al-Ghoul, KJ.; Oliver, TN.; Lane, CW.; Wodnicka, M.; Wodnicki, P. 51st Annual Meeting of the Microscopy Society of America. Cincinnati, OH, USA: San Francisco Press; 1993. Polymorphism of fiber cell junctions in mammalian lens.

Costello, MJ.; Kuszak, AJ. Chap. 23. The Types, Morphology and Causes of Cataracts. In: Garner, A.; Klintoworth, GK., editors. Pathobiology of Ocular Disease. 3rd Ed.. New York: Taylor and Francis; 2008.

Costello MJ, McIntosh TJ, Robertson JD. Membrane specializations in mammalian lens fiber cells: distribution of square arrays. Curr. Eye. Res 1985;4:1183–1201. [PubMed: 4075818]

Costello MJ, McIntosh TJ, Robertson JD. Distribution of gap junctions and square array junctions in the mammalian lens. Invest. Ophthalmol. Vis. Sci 1989;30:975–989. [PubMed: 2722452]

Costello MJ, Oliver TN, Cobo LM. Cellular architecture in age-related human nuclear cataracts. Invest. Ophthalmol. Vis. Sci 1992;33:3209–3227. [PubMed: 1399426]

Creighton MO, Trevithick JR, Mousa GY, Percy DH, McKinna AJ, Dyson C, Maisel H, Bradley R. Globular bodies: a primary cause of the opacity in senile and diabetic posterior cortical subcapsular cataracts? Can. J. Ophthalmol 1978;13:166–181. [PubMed: 698889]

Dickson DH, Crock GW. Interlocking patterns on primate lens fibers. Invest. Ophthalmol 1972;11:809–815. [PubMed: 4627255]

Dilley KJ, Bron AJ, Habgood JO. Anterior polar and posterior subcapsular cataract in a patient with retinitis pigmentosa: a light-microscopic and ultrastructural study. Exp. Eye. Res 1976;22:155–167. [PubMed: 1269540]

Dobrowolski, JA. Optical properties of films and coatings. In: Bass, M., editor. Handbooks of Optics. New York: McGraw-Hill; 1995. p. 42.1-42.109.

Fotiadis D, Hasler L, Muller DJ, Stahlberg H, Kistler J, Engel A. Surface tongue-and-groove contours on lens MIP facilitate cell-to-cell adherence. J. Mol. Biol 2000;300:779–789. [PubMed: 10891268]

Freel CD, Gilliland KO, Lane CW, Giblin FJ, Costello MJ. Fourier analysis of cytoplasmic texture in nuclear fiber cells from transparent and cataractous human and animal lenses. Exp. Eye. Res 2002;74:689–702. [PubMed: 12126943]

Garner MH, Roy D, Rosenfeld L, Garner WH, Spector A. Biochemical evidence for membrane disintegration in human cataracts. Proc Natl Acad Sci U S A 1981;78:1892–1895. [PubMed: 6785760]

Gilliland KO, Freel CD, Johnsen S, Craig Fowler W, Costello MJ. Distribution, spherical structure and predicted Mie scattering of multilamellar bodies in human age-related nuclear cataracts. Exp. Eye. Res 2004;79:563–576. [PubMed: 15381040]

Gilliland KO, Johnsen S, Metlapally S, Costello MJ, Ramamurthy B, Krishna PV, Balasubramanian D. Mie light scattering calculations for an Indian age-related nuclear cataract with a high density of multilamellar bodies. Mol. Vis 2008;14:572–582. [PubMed: 18385793]

Gonen T, Cheng Y, Kistler J, Walz T. Aquaporin-0 membrane junctions form upon proteolytic cleavage. J. Mol. Biol 2004;342:1337–1345. [PubMed: 15351655]

Gonen T, Cheng Y, Sliz P, Hiroaki Y, Fujiyoshi Y, Harrison SC, Walz T. Lipid-protein interactions in double-layered two-dimensional AQP0 crystals. Nature 2005;438:633–638. [PubMed: 16319884]

Goodenough DA. The crystalline lens. A system networked by gap junctional intercellular communication. Semin Cell Biol 1992;3:49–58. [PubMed: 1320431]

Goodenough DA, Goliger JA, Paul DL. Connexins, connexons, and intercellular communication. Annu Rev Biochem 1996;65:475–502. [PubMed: 8811187]

Hamann S, Zeuthen T, La Cour M, Nagelhus EA, Ottersen OP, Agre P, Nielsen S. Aquaporins in complex tissues: distribution of aquaporins 1–5 in human and rat eye. Am J Physiol 1998;274:C1332–C1345. [PubMed: 9612221]

Han J, Schey KL. Proteolysis and mass spectrometric analysis of an integral membrane: aquaporin 0. J Proteome Res 2004;3:807–812. [PubMed: 15359735]

Hanson SR, Hasan A, Smith DL, Smith JB. The major in vivo modifications of the human water-insoluble lens crystallins are disulfide bonds, deamidation, methionine oxidation and backbone cleavage. Exp. Eye. Res 2000;71:195–207. [PubMed: 10930324]

Harries WE, Akhavan D, Miercke LJ, Khademi S, Stroud RM. The channel architecture of aquaporin 0 at a 2.2-A resolution. Proc. Natl. Acad. Sci. USA 2004;101:14045–14050. [PubMed: 15377788]

Herpin A. Calculation of the reflecting power of any stratified system. Comptes Rendus 1947;225:182–183.

Huang L, Estrada R, Yappert MC, Borchman D. Oxidation-induced changes in human lens epithelial cells. 1. Phospholipids. Free Radic Biol Med 2006;41:1425–1432. [PubMed: 17023269]

Huang L, Grami V, Marrero Y, Tang D, Yappert MC, Rasi V, Borchman D. Human lens phospholipid changes with age and cataract. Invest Ophthalmol Vis Sci 2005;46:1682–1689. [PubMed: 15851569]

Ifeanyi F, Takemoto L. Differential binding of alpha-crystallins to bovine lens membrane. Exp Eye Res 1989;49:143–147. [PubMed: 2759187]

Ifeanyi F, Takemoto L. Specificity of alpha crystallin binding to the lens membrane. Curr Eye Res 1990;9:259–265. [PubMed: 2347203]

Jones CE, Atchison DA, Meder R, Pope JM. Refractive index distribution and optical properties of the isolated human lens measured using magnetic resonance imaging (MRI). Vis Res 2005;45:2352–2366. [PubMed: 15979462]

Jongebloed WL, Dijk F, Worst JG. Some aspects of cataract morphology: a SEM-study. Doc Ophthalmol 1988;70:155–163. [PubMed: 3234180]

Kalicharan D, Jongebloed WL, Worst JG. Lensfibre degeneration at cataract lenses. A LM, SEM and TEM investigation. Doc Ophthalmol 1993;85:77–85. [PubMed: 8181429]

Kinoshita JH, Merola LO, Satoh K, Dikmak E. Osmotic changes caused by the accumulation of dulcitol in the lenses of rats fed with galactose. Nature 1962;194:1085–1087. [PubMed: 14456182]

Kistler J, Bullivant S. The connexon order in isolated lens gap junctions. J Ultrastruct Res 1980;72:27–38. [PubMed: 7411683]

Kuck JF. Late onset hereditary cataract of the emory mouse. A model for human senile cataract. Exp Eye Res 1990;50:659–664. [PubMed: 2197106]

Kuszak, JR.; Al-Ghoul, KJ.; Costello, MJ. Pathology of age-related human cataracts. In: Tasman, WT.; Jaeger, EA., editors. Duane's Clinical Ophthalmology. vol. 71B. Philadelphia: Lippincott Williams & Wilkins; 1998. p. 1-14.

Kuszak, JR.; Costello, MJ. The Structure of the Vertebrate Lens. In: Lovicu, FJ.; Robinson, ML., editors. Development of the Ocular Lens. Cambridge, UK: Cambridge Univ. Press; 2004. p. 71-118.

Kuszak JR, Ennesser CA, Umlas J, Macsai-Kaplan MS, Weinstein RS. The ultrastructure of fiber cells in primate lenses: a model for studying membrane senescence. J. Ultrastruct. Mol. Struct. Res 1988;100:60–74. [PubMed: 3209860]

Kuszak JR, Rae JL, Pauli BU, Weinstein RS. Rotary replication of lens gap junction. J Ultrastruct Res 1982;81:249–256. [PubMed: 7143550]

Kuszak JR, Shek YH, Carney KC, Rae JL. A correlative freeze-etch and electrophysiological study of communicating junctions in crystalline lenses. Curr. Eye. Res 1985;4:1145–1153. [PubMed: 3878268]

Kuwabara T. The maturation of the lens cell: a morphologic study. Exp. Eye. Res 1975;20:427–443. [PubMed: 1126408]

Kuwabara T, Kinoshita JH, Cogan DG. Electron microscopic study of galactose-induced cataract. Invest. Ophthalmol 1969;8:133–149. [PubMed: 5777480]

Lampi KJ, Ma Z, Hanson SR, Azuma M, Shih M, Shearer TR, Smith DL, Smith JB, David LL. Age-related changes in human lens crystallins identified by two-dimensional electrophoresis and mass spectrometry. Exp. Eye. Res 1998;67:31–43. [PubMed: 9702176]

Lindsey Rose KM, Gourdie RG, Prescott AR, Quinlan RA, Crouch RK, Schey KL. The C terminus of lens aquaporin 0 interacts with the cytoskeletal proteins filensin and CP49. Invest. Ophthalmol. Vis. Sci 2006;47:1562–1570. [PubMed: 16565393]

Lizak MJ, Zigler JS Jr, Bettelheim FA. Syneretic response to incremental pressures in calf lenses. Curr. Eye Res 2005;30:21–25. [PubMed: 15875361]

Lo WK, Harding CV. Square arrays and their role in ridge formation in human lens fibers. J Ultrastruct Res 1984;86:228–245. [PubMed: 6544861]

Lo WK, Kuck JF. Alterations in fiber cell membranes of Emory mouse cataract: a morphologic study. Curr Eye Res 1987;6:433–444. [PubMed: 3581865]

Marsili S, Salganik RI, Albright CD, Freel CD, Johnsen S, Peiffer RL, Costello MJ. Cataract formation in a strain of rats selected for high oxidative stress. Exp. Eye. Res 2004;79:595–612. [PubMed: 15500819]

Metlapally S, Costello MJ, Gilliland KO, Ramamurthy B, Krishna PV, Balasubramanian D, Johnsen S. Analysis of nuclear fiber cell cytoplasmic texture in advanced cataractous lenses from Indian subjects using Debye-Bueche theory. Exp. Eye Res 2008;86:434–444. [PubMed: 18191834]

Michael R, van Marle J, Vrensen GFJM, van den Berg TJTP. Changes in the refractive index of lens fibre membranes during maturation – impact on lens transparency. Exp. Eye Res 2003;77:93–99. [PubMed: 12823992]

Murata K, Mitsuoka K, Hirai T, Walz T, Agre P, Heymann JB, Engel A, Fujiyoshi Y. Structural determinants of water permeation through aquaporin-1. Nature 2000;407:599–605. [PubMed: 11034202]

Peracchia C, Girsch SJ, Bernardini G, Peracchia LL. Lens junctions are communicating junctions. Curr. Eye. Res 1985;4:1155–1169. [PubMed: 2416512]

Pierscionek BK. Refractive index contours in the human lens. Exp. Eye Res 1997;64:887–893. [PubMed: 9301469]

Quinlan RA, Sandilands A, Procter JE, Prescott AR, Hutcheson AM, Dahm R, Gribbon C, Wallace P, Carter JM. The eye lens cytoskeleton. Eye 1999;13(Pt 3b):409–416. [PubMed: 10627818]

Schey KL, Little M, Fowler JG, Crouch RK. Characterization of human lens major intrinsic protein structure. Invest Ophthalmol Vis Sci 2000;41:175–182. [PubMed: 10634618]

Shestopalov VI, Bassnett S. Expression of autofluorescent proteins reveals a novel protein permeable pathway between cells in the lens core. J. Cell. Sci 2000;113(Pt 11):1913–1921. [PubMed: 10806102]

Shestopalov VI, Bassnett S. Development of a macromolecular diffusion pathway in the lens. J. Cell. Sci 2003;116:4191–4199. [PubMed: 12953070]

Spector A. The search for a solution to senile cataracts. Proctor lecture. Invest. Ophthalmol. Vis. Sci 1984;25:130–146. [PubMed: 6321383]

Takata T, Oxford JT, Brandon TR, Lampi KJ. Deamidation alters the structure and decreases the stability of human lens betaA3-crystallin. Biochemistry 2007;46:8861–8871. [PubMed: 17616172]

Takemoto L, Boyle D. Deamidation of alpha-A crystallin from nuclei of cataractous and normal human lenses. Mol Vis 1999;5:2. [PubMed: 10085374]

Taylor VL, Al-Ghoul KJ, Lane CW, Davis VA, Kuszak JR, Costello MJ. Morphology of the normal human lens. Invest. Ophthalmol. Vis. Sci 1996;37:1396–1410. [PubMed: 8641842]

Taylor VL, Peiffer RL, Costello MJ. Ultrastructural analysis of normal and diabetic cataractous canine lenses. Vet. & Comp. Ophthalmol 1997;7:117–125.

Tenbroek E, Arneson M, Jarvis L, Louis C. The distribution of the fiber cell intrinsic membrane proteins MP20 and connexin46 in the bovine lens. J Cell Sci 1992;103(Pt 1):245–257. [PubMed: 1331134]

Truscott RJ. Age-related nuclear cataract-oxidation is the key. Exp. Eye. Res 2005;80:709–725. [PubMed: 15862178]

Verbavatz JM, Brown D, Sabolic I, Valenti G, Ausiello DA, Van Hoek AN, Ma T, Verkman AS. Tetrameric assembly of CHIP28 water channels in liposomes and cell membranes: a freeze-fracture study. J Cell Biol 1993;123:605–618. [PubMed: 7693713]

Verkman AS. Role of aquaporin water channels in eye function. Exp Eye Res 2003;76:137–143. [PubMed: 12565800]

Vrensen G, Van Marle J, Willekens B, Van Veen H. Square arrays in early cortical opacities. Invest. Ophthalmol. Vis. Sci 1990;31:2476–2481. [PubMed: 2243013]

Vrensen G, Van Marle J, Van Veen H, Willekens B. Membrane architecture as a function of lens fibre maturation: A freeze fracture anad scanning electron microscope study in the human lens. Exp. Eye Res 1992;54:433–446. [PubMed: 1521571]

Walz T, Hirai T, Murata K, Heymann JB, Mitsuoka K, Fujiyoshi Y, Smith BL, Agre P, Engel A. The three-dimensional structure of aquaporin-1. Nature 1997;387:624–627. [PubMed: 9177353]

Weinstein, W. Vacuum. London: E. T. Heron and Co. Ltd; 1954. Computations in thin film optics; p. 3-19.

White TW, Bruzzone R. Intercellular communication in the eye: clarifying the need for connexin diversity. Brain Res Brain Res Rev 2000;32:130–137. [PubMed: 10751662]

White TW, Goodenough DA, Paul DL. Targeted ablation of connexin50 in mice results in microphthalmia and zonular pulverulent cataracts. J Cell Biol 1998;143:815–825. [PubMed: 9813099]

Yang B, Verkman AS. Water and glycerol permeabilities of aquaporins 1–5 and MIP determined quantitatively by expression of epitope-tagged constructs in Xenopus oocytes. J Biol Chem 1997;272:16140–16146. [PubMed: 9195910]

Zampighi G, Simon SA, Robertson JD, McIntosh TJ, Costello MJ. On the structural organization of isolated bovine lens fiber junctions. J. Cell. Biol 1982;93:175–189. [PubMed: 7068755]

Zampighi GA. Distribution of connexin50 channels and hemichannels in lens fibers: a structural approach. Cell Commun Adhes 2003;10:265–270. [PubMed: 14681027]

Zampighi GA, Hall JE, Ehring GR, Simon SA. The structural organization and protein composition of lens fiber junctions. J. Cell. Biol 1989;108:2255–2275. [PubMed: 2738093]

Zampighi GA, Kreman M, Lanzavecchia S, Turk E, Eskandari S, Zampighi L, Wright EM. Structure of functional single AQP0 channels in phospholipid membranes. J Mol Biol 2003;325:201–210. [PubMed: 12473462]

Zhang WZ, Augusteyn RC. On the interaction of alpha-crystallin with membranes. Curr Eye Res 1994;13:225–230. [PubMed: 8194371]

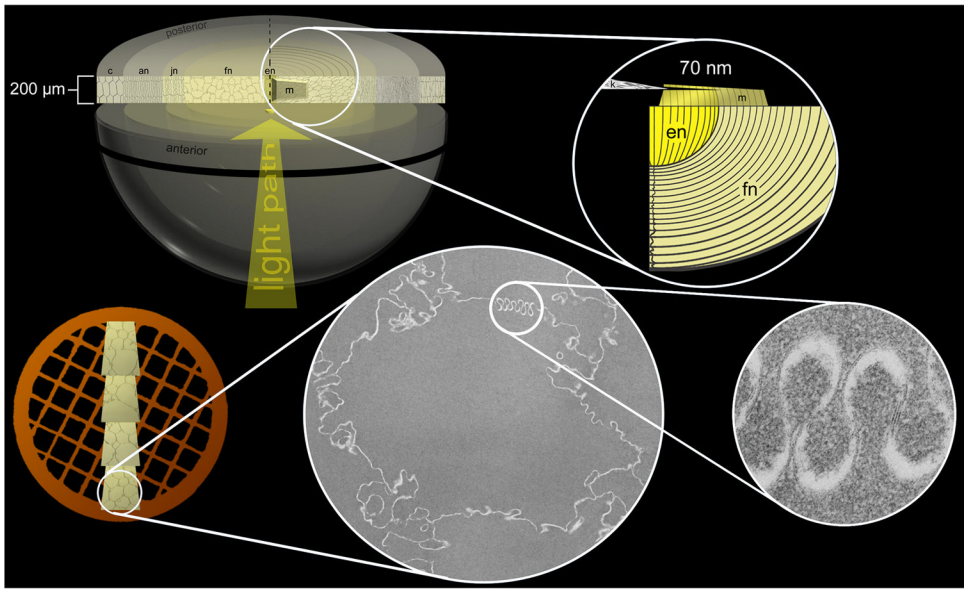

Fig. 1.

Vibratome sectioning procedure. Typically, a thick Vibratome section (200 µm) in the equatorial plane was bisected and a mesa (m) was raised near the embryonic nucleus (en) extending into the fetal nucleus (fn) (upper row). Thin sections (70 nm) were collected on copper grids, stained and examined by TEM to reveal cross-sections of fiber cells and high magnification images of membrane specializations (lower row). jn = juvenile nucleus; an = adult nucleus; c = cortex.

Fig. 2.
Photograph of a typical nucleus obtained after extracapsular extraction from a blind patient in India. The diameter was 7.5 mm indicating that nearly the entire nucleus was recovered from this probable age-related nuclear cataract (73 years old). The supporting gauze is not visible through any part of the nucleus.

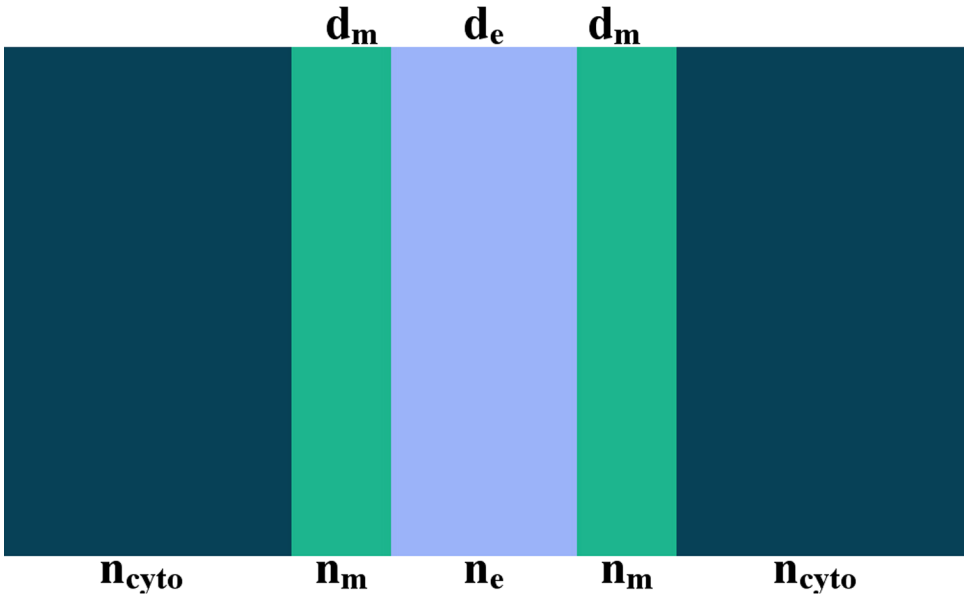

Fig. 3.

Schematic of the layers at nuclear fiber cell interfaces. The dimensions of each membrane, d_m, is 7 nm and of the ECS, d_e, is variable from 1 nm to 100 nm. As described in the text, the refractive index of the cytoplasm, n_{cyto}, is between 1.40 and 1.42, of the membranes, n_m, is higher at about 1.50 and of the ECS, n_e, is lower at about 1.35. These values can be varied to reflect aging and cataract formation.

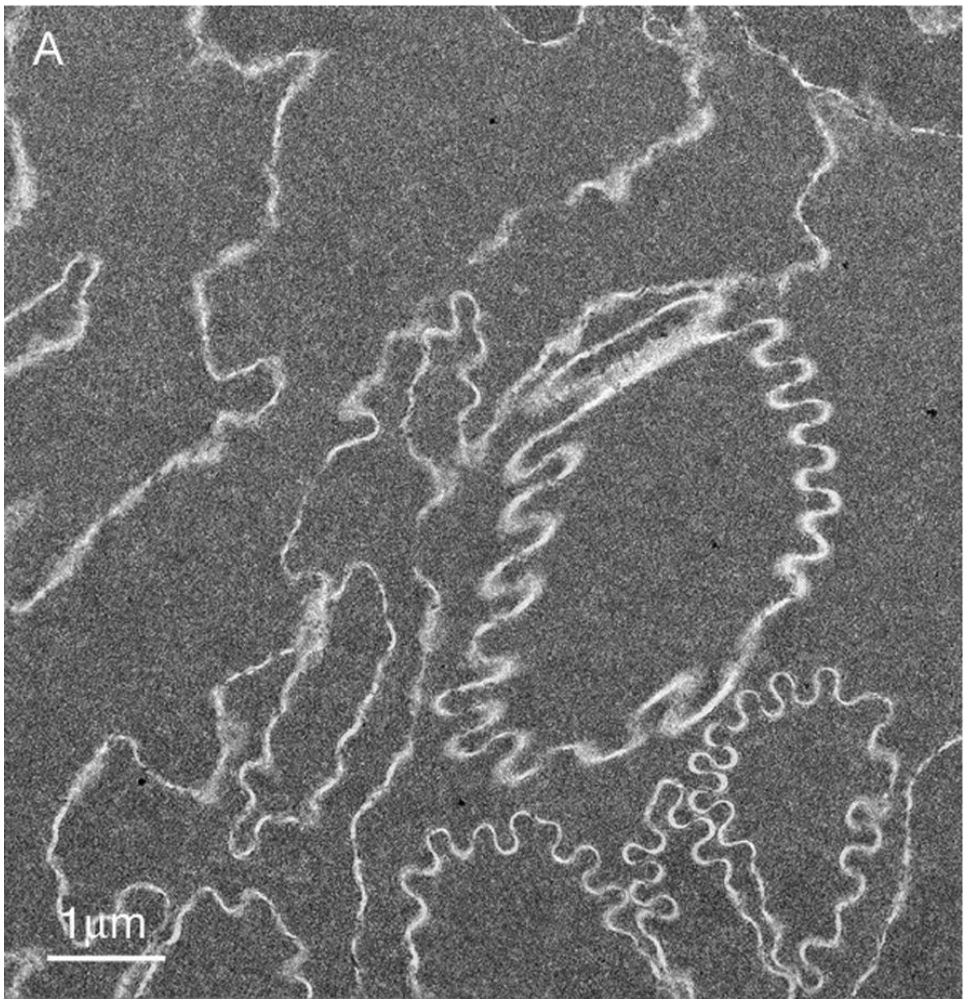

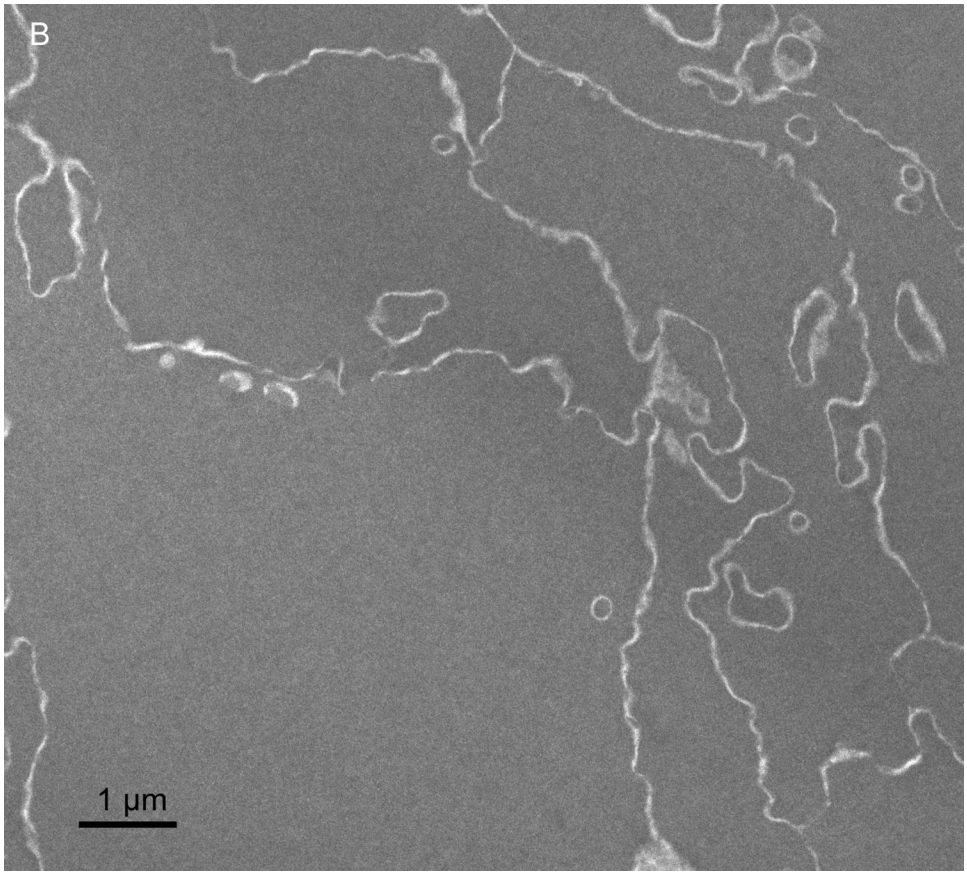

Fig. 4.

Overview TEM images of fiber cells in the lens nuclear core. (A) Fiber cells have a relatively smooth cytoplasm and membranes have a variety of curvatures with this region having an abundance of high-amplitude undulations (73 years old). (B) Similar pattern of cells and smooth cytoplasm from the nuclear core of an aged transparent donor lens with many low-amplitude undulations (56 years old).

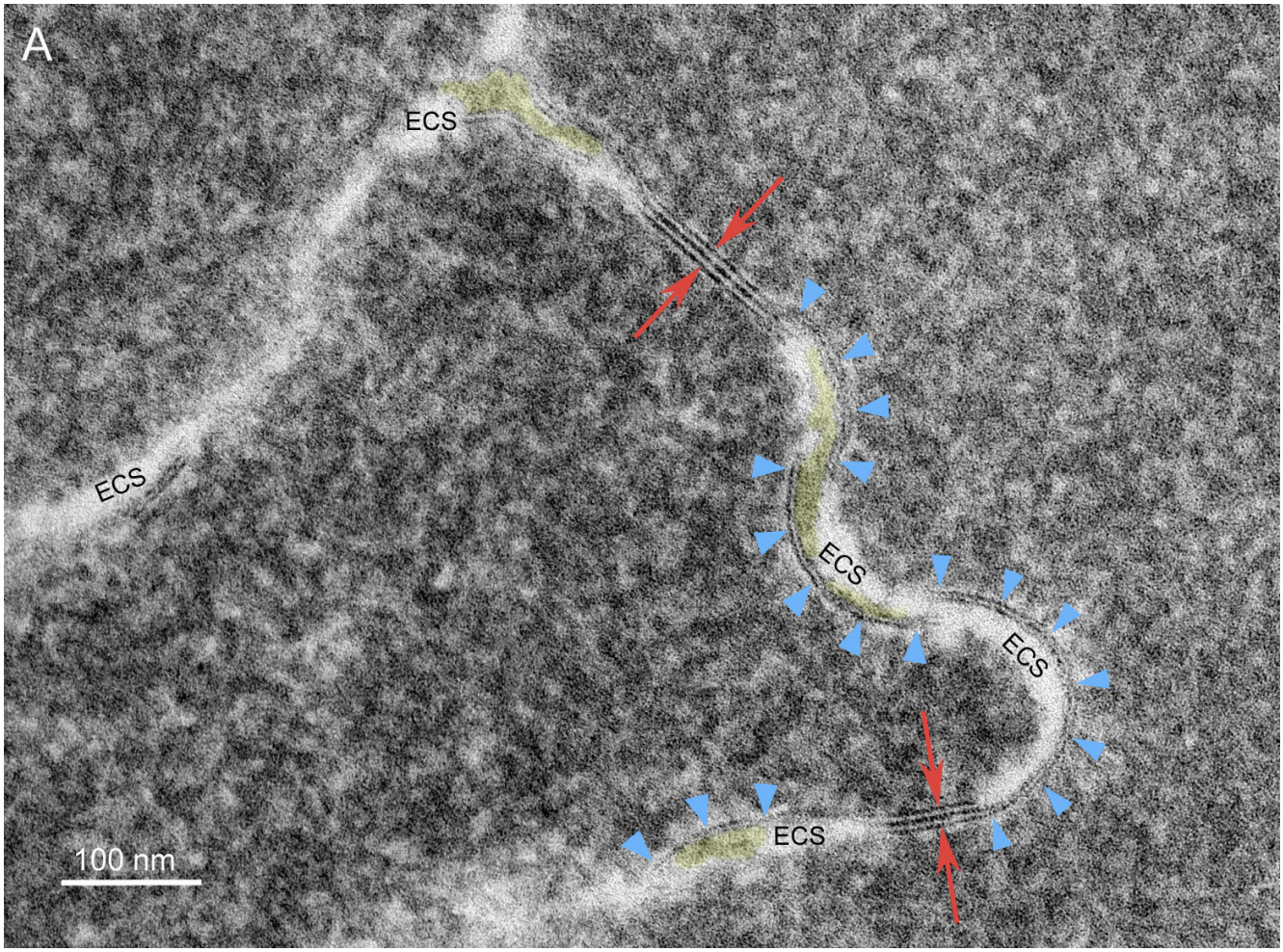

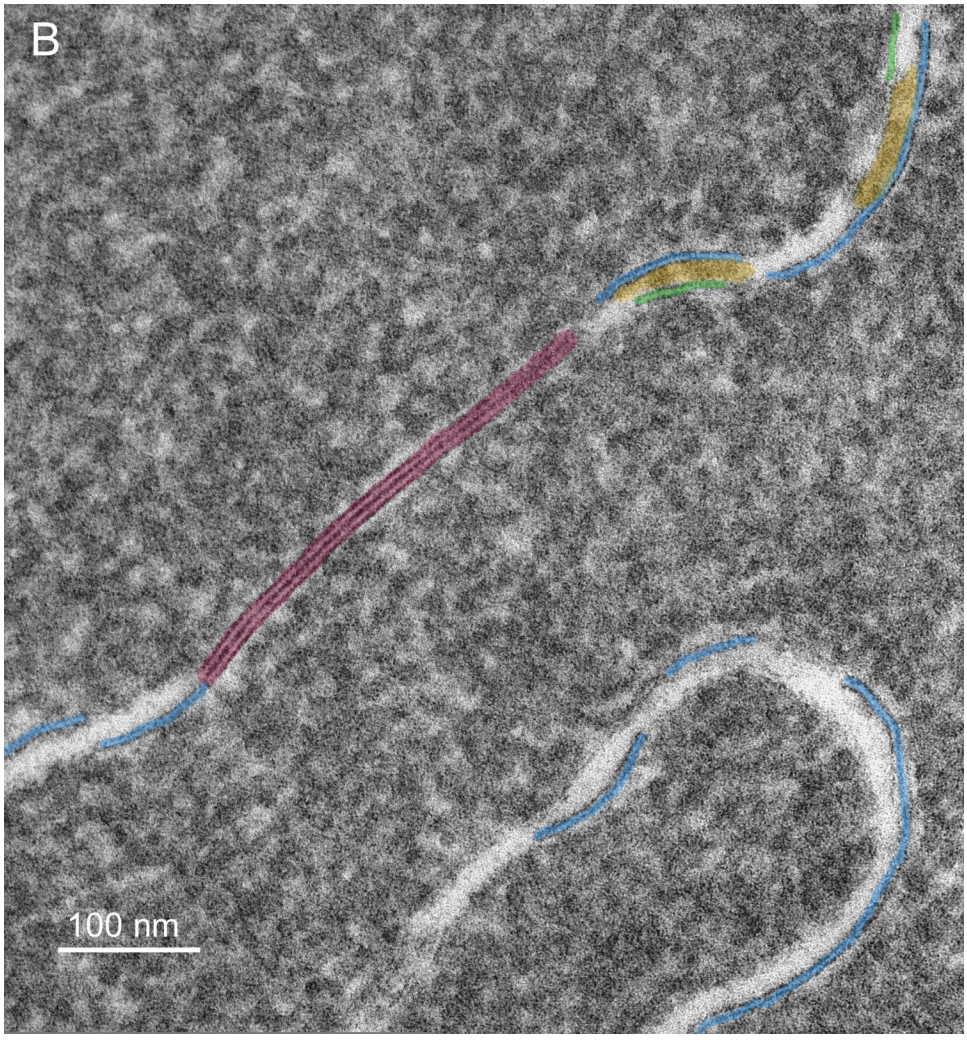

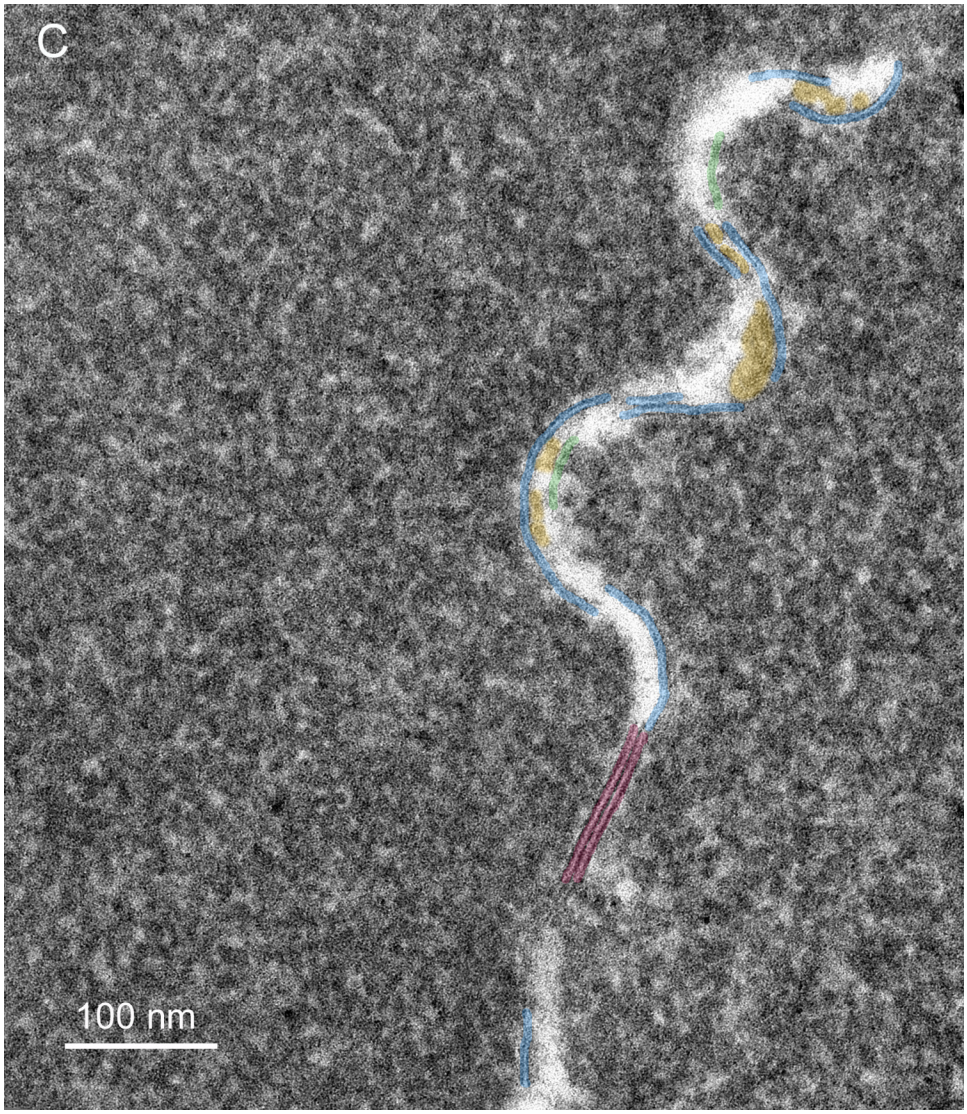

Fig. 5.

High magnification TEM images reveal membrane details in advanced nuclear cataracts. A. Individual membranes have a trilamellar profile (blue arrowheads) and junctions are pentalamellar (red arrows). The ultrastructural data indicate that bilayer membranes are lost, extracellular space (ECS) enlarges and protein-like deposits (yellow) appear, often on curved membranes containing AQP0 (blue arrowheads) (55 years old). B. Similar membrane pattern from a different advanced nuclear cataract (56 years old). Membranes and junctions are color coded as gap junctions (red lines) and aquaporin 0 containing membranes (blue lines), which predominate probably because they are the most stable. The lipid-rich bilayers (green lines) define the ECS where protein-like deposits (yellow) are frequently observed. C. High magnification TEM image of membranes from a transparent donor lens (48 years old). Membranes are colorized as in Fig. 5B. Notice that the membranes are similar and the cytoplasm is more homogeneous compared to images of the cataracts.

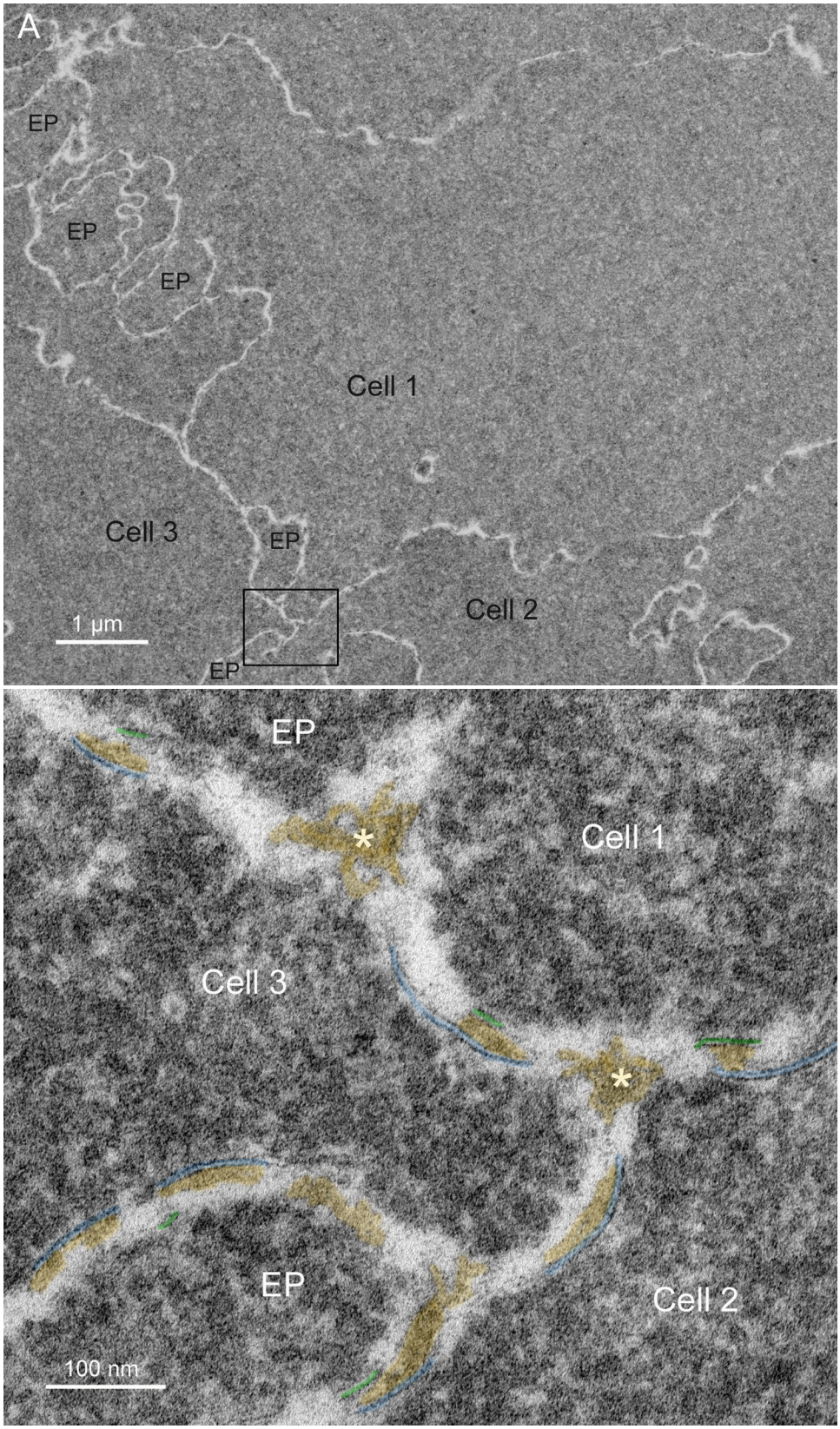

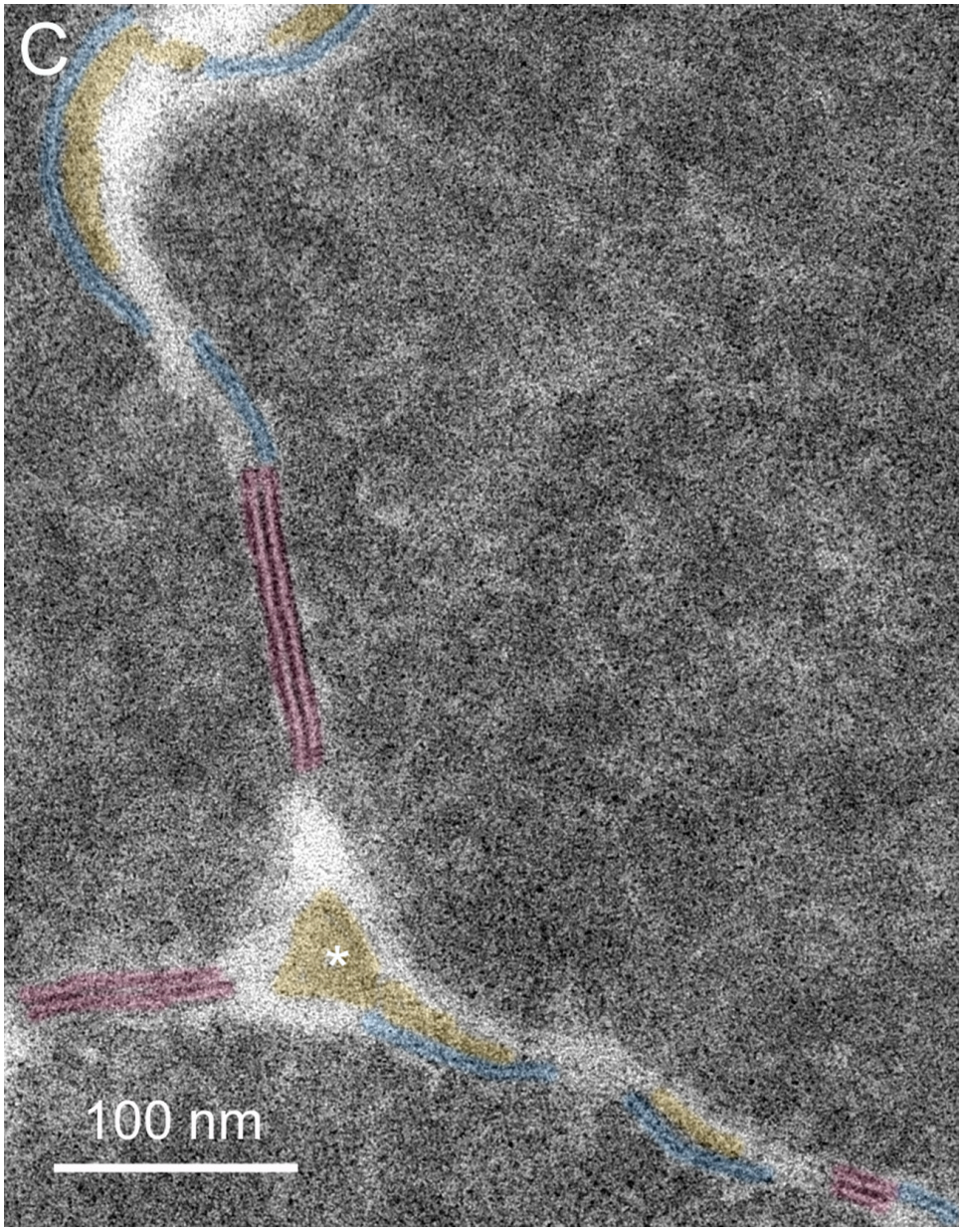

Fig. 6.

Membranes at cell-cell and cell-process intersections. A. Overview of three cells shows a typical pattern of cellular architecture in a mature nuclear cataract. Numerous edge processes (EP) are displayed at the interfaces of adjacent cells (51 years old). B. High magnification of one region (boxed in A) reveals damaged membranes from three cells and two edge processes. Extracellular space deposits (yellow) appear on curved membranes (blue and green lines) and similarly staining material occurs at trigonal intersections (*). The trigonal points are extended extracellular channels that are partially filled with protein-like material. C. A trigonal intersection in which the protein-like material is triangular in shape (*) and the adjacent membranes and junctions are distinct (70 years old).

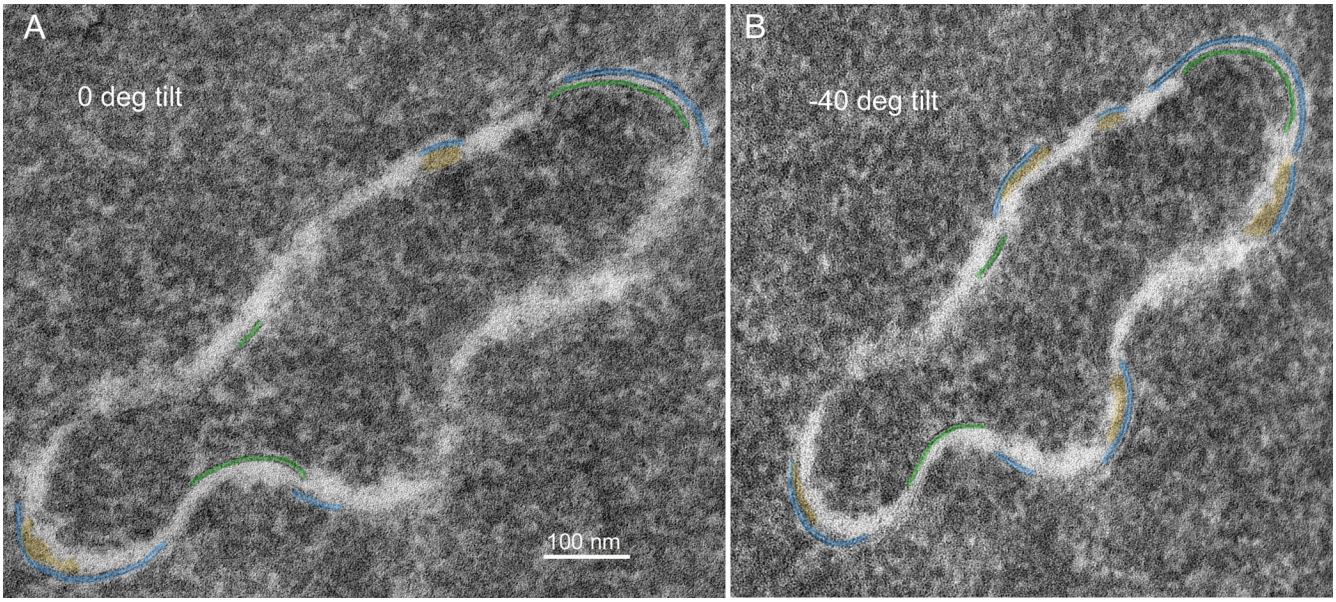

Fig. 7.

Finger-like process viewed at different tilts exposes different regions of preserved membranes (73 years old). A. At 0° tilt, the percentage of the perimeter displaying at least one membrane is 48%. Some ECS deposits are noted (yellow) on the concave side of curved membranes. Other dark staining material may also be deposits but the membranes are not visible. B. Tilting the grid to 40° (counterclockwise) exposes more membranes, now measuring about 65% of the perimeter. More ECS deposits are also indicated. The tilt axis is vertical, thus the finger-like process appears proportionally shorter in projection.

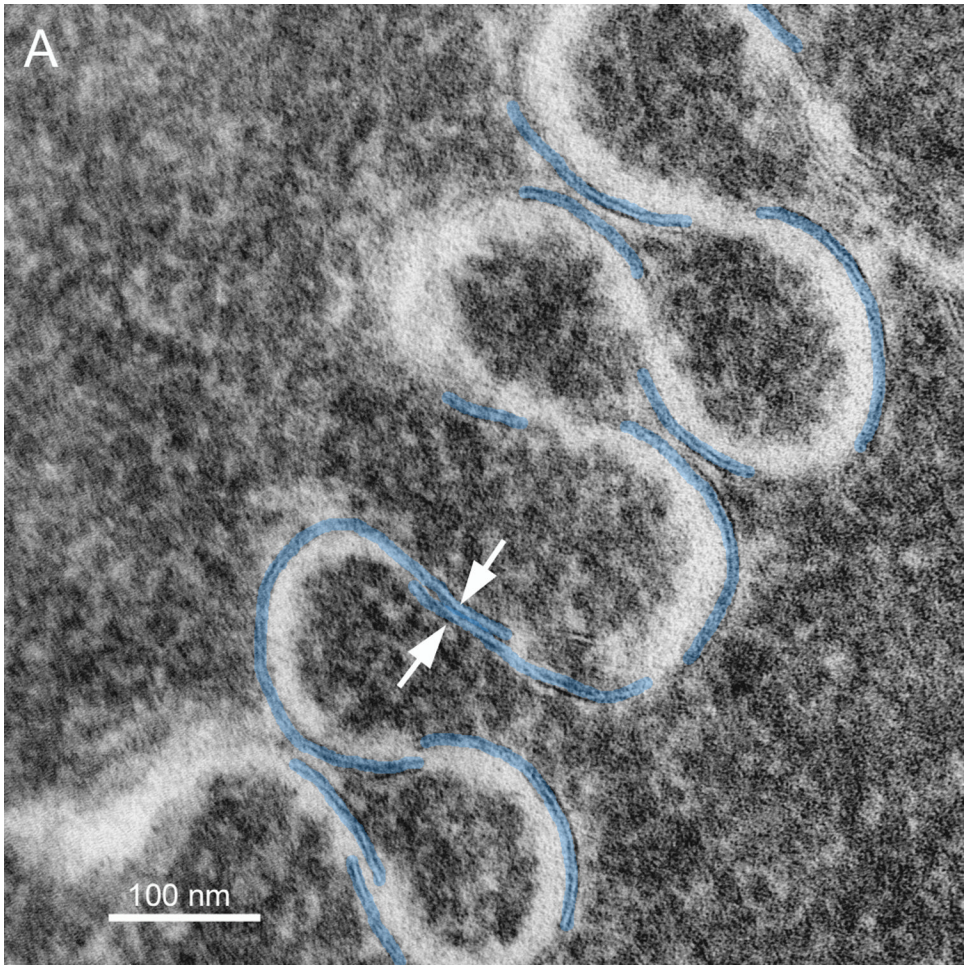

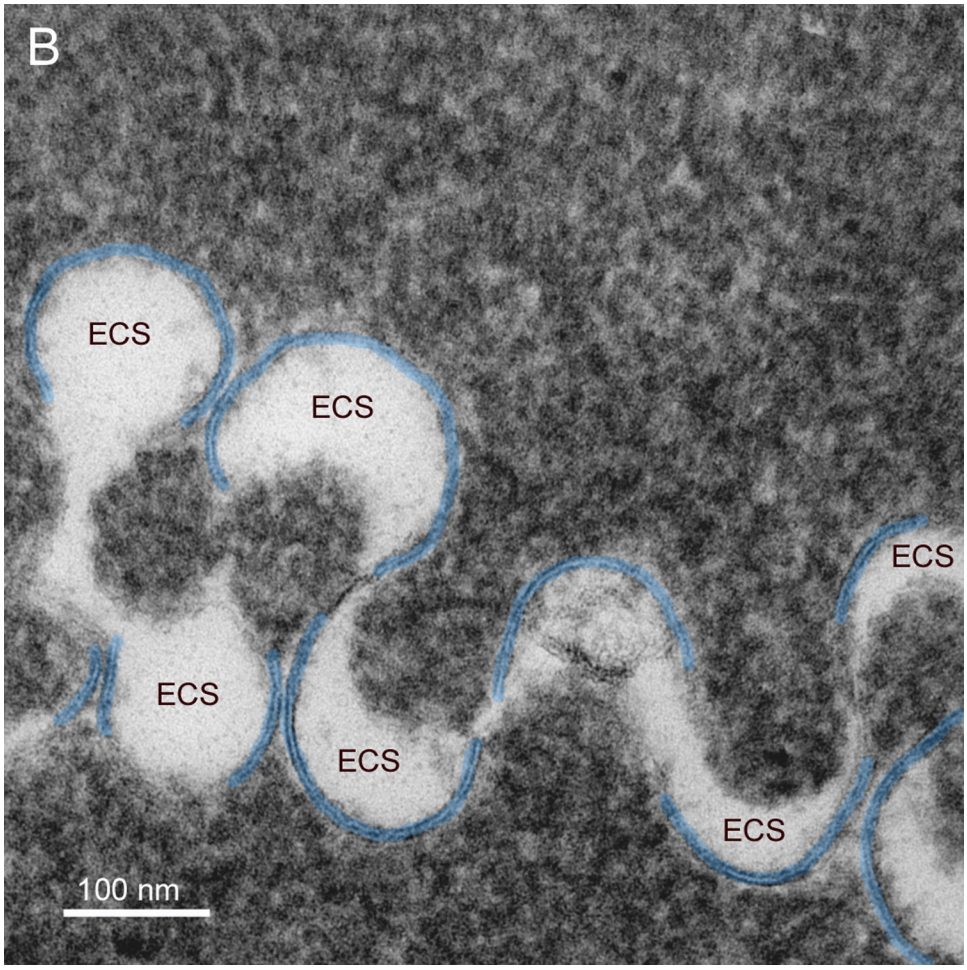

Fig. 8.

Highly undulating membranes show distinctive patterns. A. Undulating membranes with high amplitude have curved membranes that overlap at transitions in curvature. The overlap at 40° tilt (counterclockwise) can be seen to form symmetric junctions similar in appearance to gap junctions but about 2 nm thinner (arrows). It is often necessary to tilt the grid through ±50° to bring the junction into optimum position for viewing and measurement (38 years old). B. The extracellular space (ECS) within some undulating membranes can be enlarged. At the proper tilt, the membrane profiles are clear and the ECS, which is cylindrical with an irregular cross-section, is visualized in cross-section. The size of the ECS can be greater than 100 nm and thus these low-density cylinders could contribute to increased light scattering (73 years old).

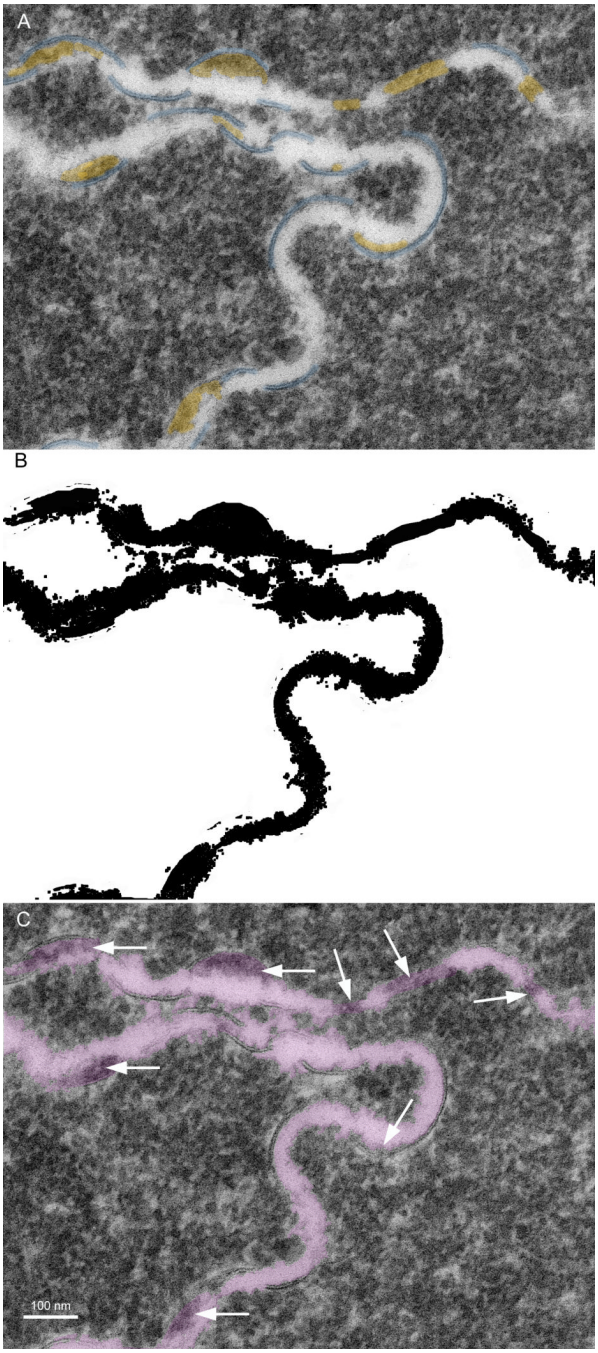

Fig. 9.

Morphometric analysis to determine the average thickness of the ECS. A. TEM image of a cataract showing well-defined membranes (blue) and ECS deposits (yellow) (51 years old). B. ECS after automatic threshold processing, inverting and manual removal of non-ECS pixels. The total number of ECS pixels was equivalent to about 120,000 nm^2 and the length of the ECS measured about 2800 nm. Therefore, the average thickness of the ECS for this example was about 42 nm. C. Overlay of images, with the threshold derived ECS colored and at 20% transparency, indicating the close correspondence of processed and original ECS. The ECS deposits appear darker and are easy to locate (arrows).

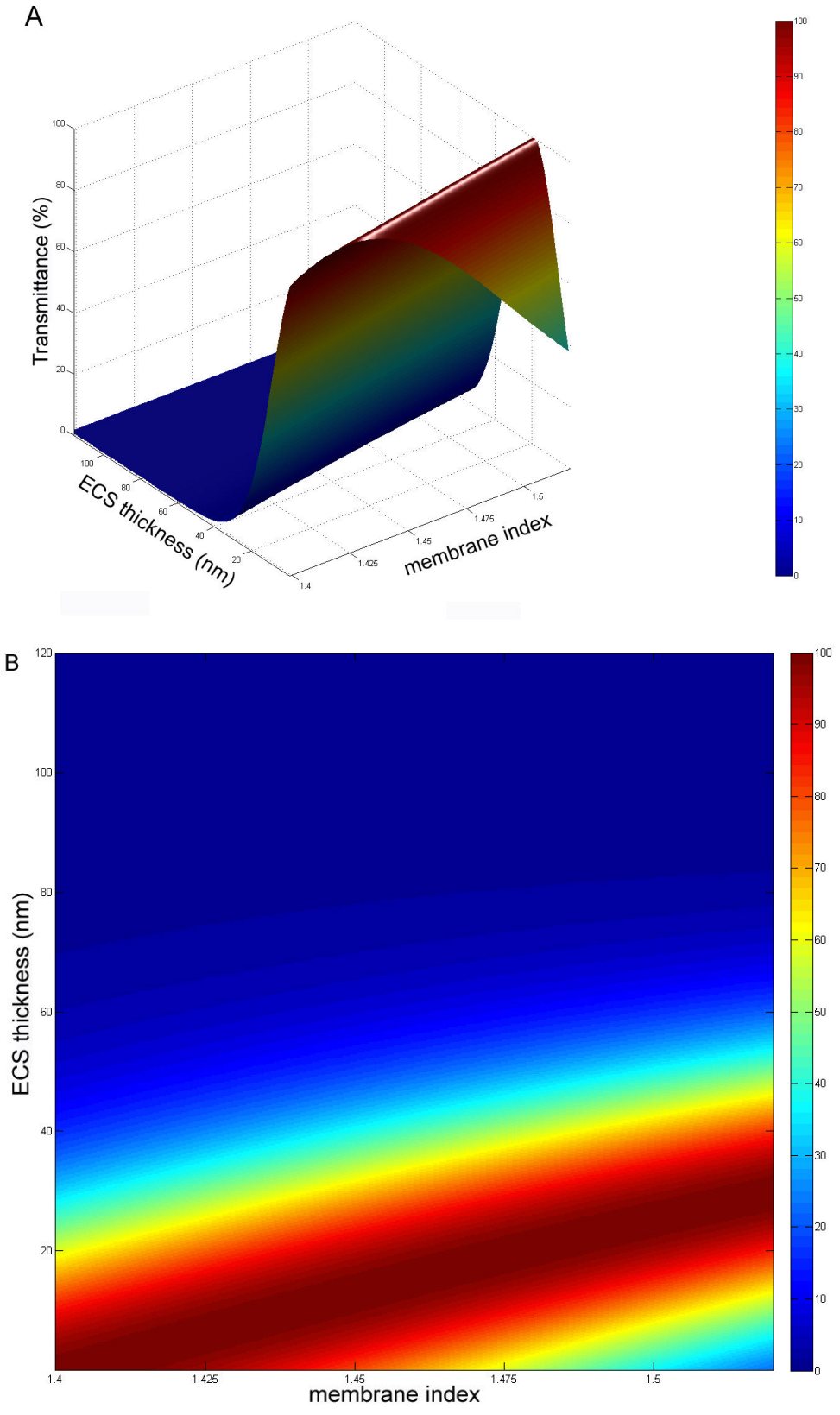

Fig. 10.

Theoretical calculation of the percent transmittance for a nucleus containing 4000 membrane interefaces with layers as described in Fig. 3. A. Surface plot for n_{cyto} = 1.42 and n_e = 1.35. Nearly 100% transmittance is predicted for ECS thicknesses of 15 – 20 nm for n_m = 1.50. B. Flat projection view for the same conditions in A except for n_{cyto} = 1.40. Note that the 100% transmittance at n_m = 1.50 occurs at about 25–30 nm and that there is a very steep drop in transmittance above 35 nm.

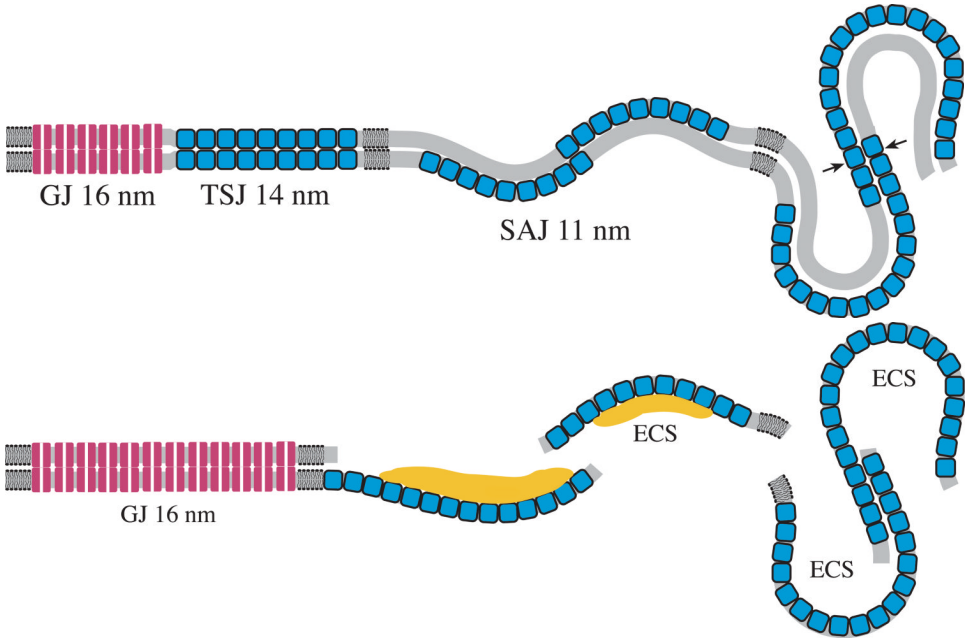

Fig. 11.

Diagrams illustrating hypothesized molecular interpretations of observed membrane patterns. A. Paired membranes of adjacent fiber cells adopt various junctional associations depending on the developmental zone. Gap junctions are found consistently throughout the lens as 16 nm thick symmetrically stained profiles (red cylinders, representing connexons with aligned white channels). Thinner symmetrically stained junctions, about 14 nm thick and probably composed of AQP0 tetramers (blue squares), are found mostly in the cortex. Undulating membrane pairs contain single membranes of AQP0 that stain asymmetrically when paired with lipid-rich bilayers and are found throughout the nucleus at low amplitude, where the closest association is about 11 nm, and in the nuclear core at high amplitude. At cross-over points (transitions in curvature) the AQP0 membranes are hypothesized to pair to form an adhesive junction (arrows). GJ = gap junction; TSJ = thin symmetric junction; SAJ = square-array junction. Redrawn from Kuszak and Costello, 2004. B. Membrane damage in paired membranes of the nucleus. Extensive gap junctions are observed in all developmental regions within the nucleus. Undulating membranes predominate, mainly with low amplitude. Loss of the lipid-rich bilayers (gray) and enlarged extracellular spaces (ECS) are common. Protein-like deposits in the ECS (yellow) are observed frequently on curved membranes containing arrays of AQP0. Pockets of ECS with low stain density can occur within high-amplitude undulating membranes.